Biophysical Journal
Article

Biophysical Society

tRNA Fluctuations Observed on Stalled Ribosomes Are Suppressed during Ongoing Protein Synthesis

Ryan M. Jamiolkowski,[1] Chunlai Chen,[1,2,*] Barry S. Cooperman,[3,*] and Yale E. Goldman[1,*]
[1]Pennsylvania Muscle Institute, Perelman School of Medicine at the University of Pennsylvania, Philadelphia, Pennsylvania; [2]School of Life Sciences, Tsinghua-Peking Joint Center for Life Sciences, Beijing Advanced Innovation Center for Structural Biology, Tsinghua University, Beijing, China; and [3]Department of Chemistry, University of Pennsylvania, Philadelphia, Pennsylvania

ABSTRACT The pretranslocation complex of the ribosome can undergo spontaneous fluctuations of messenger RNA and transfer RNAs (tRNAs) between classical and hybrid states, and occupation of the hybrid tRNA positions has been proposed to precede translocation. The classical and hybrid state tRNA positions have been extensively characterized when the ribosome is stalled along the messenger RNA by either the absence or delayed addition of elongation factor G (EF-G), or by the presence of antibiotics or GTP analogs that block translocation. However, during multiple ongoing elongation cycles when both EF-G and ternary complexes are present, EF-G can bind to the pretranslocation complex much faster than the timescale of the classic-hybrid transitions. Using single-molecule fluorescence resonance energy transfer between adjacent tRNAs and between A-site tRNA and ribosomal protein L11, we found that the tRNAs do not fluctuate between the hybrid and classical states, but instead adopt a position with fluorescence resonance energy transfer efficiencies between those of the stalled classical and hybrid states.

INTRODUCTION

During protein synthesis, transfer RNAs (tRNAs) successively occupy three positions on the ribosome: A (aminoacyl), P (peptidyl), and E (exit) sites. After an aminoacylated tRNA enters the A site, a new peptide bond is formed as the nascent peptide chain is transferred from the P-site tRNA to the A-site tRNA. The resulting pretranslocation (PRE) complex of the ribosome undergoes elongation factor G (EF-G)-catalyzed translocation (1–5) to a posttranslocation (POST) complex, which shifts the messenger RNA (mRNA) by one three-base codon relative to the ribosome, and moves the tRNAs from the A and P sites to the P and E sites, respectively. Binding of the next aminoacylated tRNA into the A site initiates a subsequent cycle of elongation. The PRE complex formed by ribosomes stalled in the absence of EF-G fluctuates between so-called "classical" and "hybrid" states (6–8).

In these earlier works, the structural distinction between classical and hybrid states was focused on the tRNA positions within the ribosome's active site: "classical" tRNA positions referred to the A/A and P/P locations of bound tRNAs, where the first and second letters represent binding sites on the 30S and 50S subunits, respectively, and a canonical hybrid state, in which tilted tRNAs bound in mixed A/P and P/E positions. The hybrid state was proposed to be an intermediate between the classical PRE state and the POST complex in which the tRNAs are bound at P/P and E/E sites. Concurrent and subsequent structural studies showed that EF-G catalysis of tRNA-mRNA translocation was also accompanied by large-scale motions within the ribosome as a whole, including 6° (9) to 9° (10,11) rotations of the 30S subunit with respect to the 50S subunit, and of the head region of the 30S subunit relative to its body (12,13). These studies were supported by fluorescence resonance energy transfer (FRET) measurements in both single-molecule (14–24) and ensemble (25,26) experiments. Further structural studies identified additional distinct states of the PRE complex containing tRNAs in somewhat different and/or intermediate locations from the canonical hybrid A/P and P/E sites, which have been identified as ap/ap:pe/E (27), ap/P:pe/E (28), and A/P*:P/E (12).

It was proposed that tRNA tilting, rotations of the large and small subunits, and motions of protein L1 could be considered as coupled, defining two main global states: classical states with unrotated large and small subunits and nontilted tRNAs, and hybrid states with rotated subunits and tilted tRNAs (29). However, more recent evidence demonstrates that tRNA tilting, subunit rotations, and L1 stalk motions

Submitted April 11, 2017, and accepted for publication August 30, 2017.
*Correspondence: chunlai@biomed.tsinghua.edu.cn or cooprman@pobox.upenn.edu or goldmany@upenn.edu
Editor: Karin Musier-Forsyth.
https://doi.org/10.1016/j.bpj.2017.08.052

are temporally distinct processes (18,25,26,30) that are not tightly coupled.

Before the work presented here, single molecule fluorescence resonance energy transfer (smFRET) studies that monitored changes in tRNA positions during EF-G-catalyzed translocation have been conducted mainly by adding EF-G to stalled PRE complexes, formed in the absence of EF-G, that were equilibrated between the classical and canonical hybrid states, with a significant fraction displaying reversible fluctuations between these two states (13,21,31–34). These studies supported the notion that the classical-hybrid transition in PRE complexes plays an important role during translocation. One study that did observe multicodon elongation with EF-G present in the solution (22) observed extremely slow fluctuations in the PRE state, but monitored subunit rotations rather than tRNA positions.

Once EF-G binds to the ribosome, tRNA and subunit fluctuations diminish or stop (21,22). Our recent study employing smFRET to monitor ongoing translation of a full-length protein gave results indicating that A-site-bound peptidyl-tRNA in PRE complexes did not fluctuate and had, at most, a minor fraction (<6%) in the hybrid position (35). This result raised the interesting question of whether the translocation pathway during ongoing polypeptide synthesis might differ in important ways from the translocation pathway resulting from EF-G addition to stalled PRE complexes. However, it did not resolve that question because it employed a time resolution similar to the measured rate of classical-hybrid tRNA fluctuations (which could have prevented their detection) and at one EF-G·GTP concentration.

In this work, we overcome these limitations in studying elongation in ribosomes that are not stalled. We use smFRET between two ribosome-bound tRNAs, and between a tRNA and L11, a ribosomal protein located near the A site, to monitor translocation during ongoing translation of a model polypeptide at much higher time resolution, at varying levels of EF-G·GTP, and during the synthesis of peptides of various lengths (dipeptide, tripeptide, hexapeptide, heptapeptide). These results show that an EF-G·GTP concentration of 2 μM is sufficient to rapidly place an incoming tRNA in a position between the canonical classical and hybrid states before its translocation into the P site. We discuss differences in our results from those of previous studies, and the implications of our work for translocation within cells.

MATERIALS AND METHODS

In brief, 70S initiation complexes were formed using a 5′-biotinylated mRNA (Dharmacon RNAi Tech; sequences in Supporting Materials and Methods), and fluorescence-labeled ternary complexes (TCs) were preformed from elongation factor thermo unstable (EF-Tu), GTP, and charged tRNAs labeled with either Cy3 or Cy5 at dihydrouridine positions in the D loop (36). For stalled experiments, the unlabeled TCs, (as well as the labeled Phe TC in the particular case of tRNA-tRNA FRET experiments), 2 μM EF-G, and 3 mM GTP were added to the initiation complexes and incubated for 5 min, followed by immobilization of the resulting POST complexes on a streptavidin/biotin-PEG-coated glass surface (21,37). Unbound reaction components including EF-G were then washed out of the channel. Labeled Val TC was then added in the absence of EF-G to form a new PRE complex, with image stacks recorded either during the addition or after washing away unbound labeled TCs. For ongoing experiments, the initiation complexes alone were immobilized on the slide, and all cognate TCs (labeled and unlabeled) were added in the presence of 2 μM EF-G and 3 mM GTP during recording.

Cy3 and Cy5 fluorescence intensities (allowing calculation of FRET between Cy3 and Cy5) were collected using the alternating laser excitation (ALEX) mode to switch between 532 nm and 640 nm lasers on an objective-type total internal reflection fluorescence microscope (21). Except as otherwise indicated, stalled experiments were recorded with ALEX at 35 ms integration time per frame, resulting in a net time resolution of 70 ms, whereas ongoing translation experiments were recorded solely with 532 nm excitation, giving 35 ms time resolution. Most translation experiments were carried out with buffer TAM_{15} (15 mM $MgAc_2$, 50 mM Tris-HCl (pH 7.5), 30 mM NH_4Cl, 70 mM KCl, and 1 mM DTT) at 23°C. More extensive details of materials preparation, the experimental setup, FRET measurements, alternative buffers, swapped labels, and data analysis are described in the Supporting Materials and Methods.

RESULTS

Labeled complexes

We examined the dynamics of FRET between A-site tRNA and L11 or between adjacent tRNAs in the A- and P-sites, or P- and E-sites, during ongoing polypeptide elongation experiments when EF-G is continuously present from the start of elongation. For this purpose, we used ribosomes programmed with mRNA-6,7 (Table 1) and four fluorescence-labeling schemes: A) Val-$tRNA^{Val}$(Cy3) and Cy5-L11 [denoted V^7(Cy3)-L11(Cy5)], B) Phe-$tRNA^{Phe}$(Cy5) and Val-$tRNA^{Val}$(Cy3) [F^6(Cy5)-V^7(Cy3)], C) Phe-$tRNA^{Phe}$(Cy3) and Val-$tRNA^{Val}$(Cy5) [F^6(Cy3)-V^7(Cy5)], and D) Phe-$tRNA^{Phe}$(Cy3) and Cy5-L11 [F^6(Cy3)-L11(Cy5)]. Experiments on ribosomes programmed with mRNA-2,3 tested dynamics of FRET between A-site bound tRNA and L11 earlier in elongation with three labeling schemes: E) Val-$tRNA^{Val}$(Cy3) and Cy5-L11 [V^3(Cy3)-L11(Cy5)], F) Val-$tRNA^{Val}$(Cy5) and Cy3-L11 [V^3(Cy5)-L11(Cy3)], and G) and Phe-$tRNA^{Phe}$(Cy3) and Cy5-L11 [F^2(Cy3)-L11(Cy5)].

smFRET in stalled PRE complexes

Stalled PRE complexes formed in the absence of EF-G·GTP displayed high and low values for both tRNA-L11 FRET and tRNA-tRNA FRET, associated with the classical and hybrid tRNA positions, respectively, consistent with previous work by ourselves and others (8,21,23,31) and observed with labeling schemes A–G. To examine the stalled V^7(Cy3)-L11(Cy5) (labeling scheme A, Fig. 1, *A–C*) and F^6(Cy5)-V^7(Cy3) (labeling scheme B, Fig. 2, *A–C*) Val-$tRNA^{Val}$(Cy3) states, TC was added to a sample containing stalled POST-6 complexes (with P-site bound fMYYYYF-$tRNA^{Phe}$) in the absence of EF-G, forming the stalled PRE-7 complex. FRET efficiency distribution for each

TABLE 1 Summary of smFRET results

mRNA	Labeling scheme	Fluorescent Labeling Scheme														FRET Pair	FRET Efficiencies: Stalled-PRE Classic	FRET Efficiencies: Stalled-PRE Hybrid	FRET Efficiencies: $INT_{ongoing}$	$(E_{ongoing} - E_{hybrid})/(E_{classical} - E_{hybrid})$
mRNA-6,7	A	AUG	UAU	UAU	UAU	UAU	UUC	GUG	CGU	UAU	UAU	UAU	UAU	UAU		V^7(Cy3)-*L11(Cy5)*	0.73 ± 0.01 (Fig 1C)	0.49 ± 0.02 (Fig 1C)	0.65 ± 0.01 (Fig 1F)	0.67
		fMet	Tyr	Tyr	Tyr	Tyr	Phe	Val	Arg	Tyr	Tyr	Tyr	Tyr	Tyr						
		1	2	3	4	5	6	7	8	9	10	11	12	13						
	B	AUG	UAU	UAU	UAU	UAU	*UUC*	GUG	CGU	UAU	UAU	UAU	UAU	UAU		*F^6(Cy5)*-V^7(Cy3)	0.68 ± 0.01 (Fig 2C)	0.39 ± 0.01 (Fig 2C)	0.58 ± 0.01 (Fig 2F)	0.66
		fMet	Tyr	Tyr	Tyr	Tyr	*Phe*	Val	Arg	Tyr	Tyr	Tyr	Tyr	Tyr						
		1	2	3	4	5	*6*	7	8	9	10	11	12	13						
	C	AUG	UAU	UAU	UAU	UAU	UUC	*GUG*	CGU	UAU	UAU	UAU	UAU	UAU		F^6(Cy3)-*V^7(Cy5)*	0.73 ± 0.01 (Fig S1C)	0.40 ± 0.01 (Fig S1C)	0.57 ± 0.02 (Fig S1F)	0.52
		fMet	Tyr	Tyr	Tyr	Tyr	Phe	*Val*	Arg	Tyr	Tyr	Tyr	Tyr	Tyr						
		1	2	3	4	5	6	*7*	8	9	10	11	12	13						
	D	AUG	UAU	UAU	UAU	UAU	UUC	GUG	CGU	UAU	UAU	UAU	UAU	UAU		F^6(Cy3)-*L11(Cy5)*	0.73 ± 0.01 (Fig S2C)	0.43 ± 0.01 (Fig S2C)	0.69 ± 0.01 (Fig S2F)	0.87
		fMet	Tyr	Tyr	Tyr	Tyr	Phe	Val	Arg	Tyr	Tyr	Tyr	Tyr	Tyr						
		1	2	3	4	5	6	7	8	9	10	11	12	13						
mRNA-2,3	E	AUG	UUC	GUG	CGU	UAU	UAU	UAU	UAU	UAU	UAU	UAU	UAU	UAU		V^3(Cy3)-*L11(Cy5)*	0.73 ± 0.01 (Fig S1J)	0.46 ± 0.02 (Fig S1J)	0.66 ± 0.01 (Fig S1M)	0.74
		fMet	Phe	Val	Arg	Tyr	Tyr	Tyr	Tyr	Tyr	Tyr	Tyr	Tyr	Tyr						
		1	2	3	4	5	6	7	8	9	10	11	12	13						
	F	AUG	UUC	*GUG*	CGU	UAU	UAU	UAU	UAU	UAU	UAU	UAU	UAU	UAU		*V^3(Cy5)*-L11(Cy3)	0.70 ± 0.01 (Fig S1Q)	0.49 ± 0.03 (Fig S1Q)	0.63 ± 0.02 (Fig S1T)	0.67
		fMet	Phe	*Val*	Arg	Tyr	Tyr	Tyr	Tyr	Tyr	Tyr	Tyr	Tyr	Tyr						
		1	2	*3*	4	5	6	7	8	9	10	11	12	13						
	G	AUG	UUC	GUG	CGU	UAU	UAU	UAU	UAU	UAU	UAU	UAU	UAU	UAU		F^2(Cy3)-*L11(Cy5)*	0.74 ± 0.01 (Fig S2L)	0.43 ± 0.01 (Fig S2L)	0.68 ± 0.01 (Fig S2O)	0.81
		fMet	Phe	Val	Arg	Tyr	Tyr	Tyr	Tyr	Tyr	Tyr	Tyr	Tyr	Tyr						
		1	2	3	4	5	6	7	8	9	10	11	12	13						

mRNA-6,7 and mRNA-2,3 displayed in the table were used to program unlabeled ribosomes (B and C), L11(Cy5) ribosomes (A, D, E, and G), and L11(Cy3) ribosomes (F) for smFRET experiments using the FRET pairs listed in the table, corresponding to the italicized (Cy5) or underlined (Cy3) codons in the sequences. PRE complexes were stalled by the absence of EF-G and used to form two-peaked FRET distributions fit with a double Gaussian function, giving the high and low FRET peaks corresponding to the classical and hybrid tRNA positions. The peak centers from aggregated data, as well as SEs of the peaks from multiple replicate experiments, are displayed in the table. Experiments were also conducted during ongoing translation in the presence of 2 μM EF-G, which yielded single-peaked FRET distributions of aggregate data, whose values are displayed in the table along with SEs from multiple replicate experiments. The single peaks (corresponding to $INT_{ongoing}$) had FRET efficiencies in between the stalled classical and hybrid values, as expressed in the ratio $(E_{ongoing} - E_{hybrid})/(E_{classical} - E_{hybrid})$.

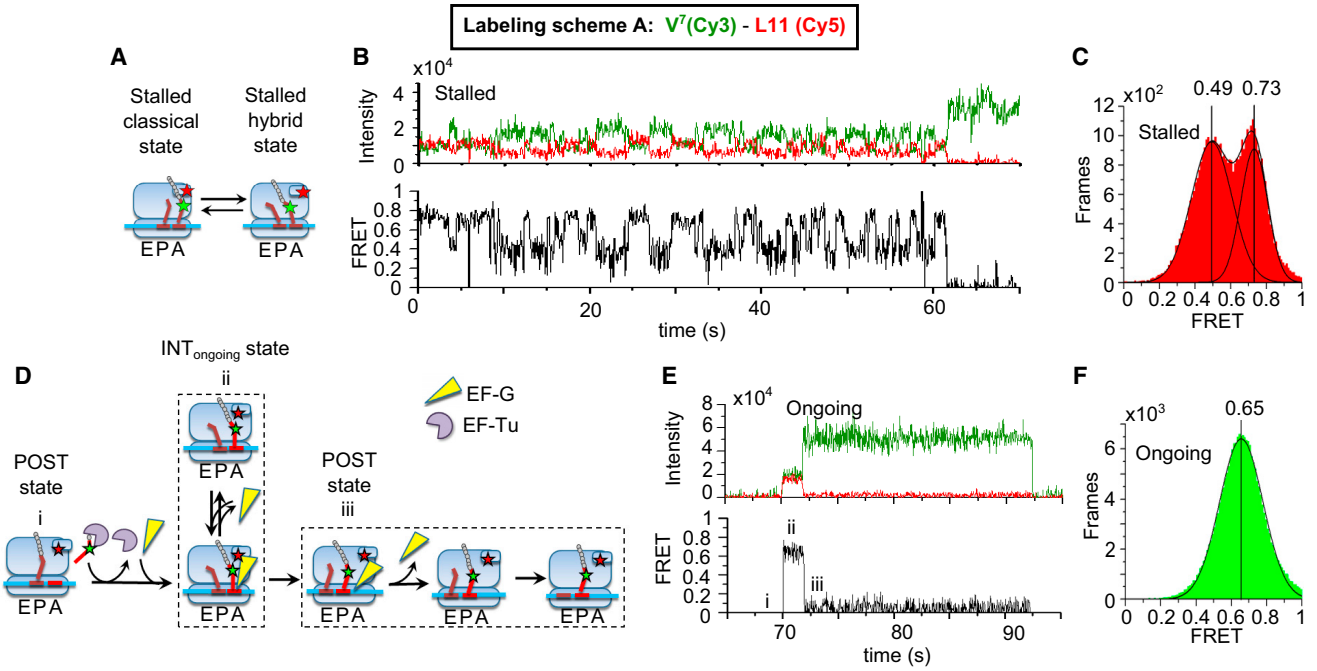

FIGURE 1 Stalled and ongoing tRNA-L11 FRET measurements. L11(Cy5) ribosomes were programmed with mRNA-6,7 (Table 1) and underwent FRET with Val-tRNA^{Val}(Cy3). (*A*) Schematic of classical/hybrid equilibrium of a stalled ribosome. The green and red stars represent Cy3 fluorophore and Cy5 fluorophore, respectively. (*B*) Representative FRET recording. (*C*) Frames of fluctuating stalled traces formed a two-peaked distribution fit with a double Gaussian function ($n = 592$ molecules). (*D–F*) 2 μM EF-G was present during ongoing translation from codons 1–7. (*D*) Reaction scheme for ongoing translation. (*E*) A representative trace with the following FRET states: i) the POST state after the ribosome has translated through the fifth (Tyr) and sixth (Phe) codons, with peptidyl-tRNA^{Phe} residing in the P site; ii) INT$_{ongoing}$; and iii) the POST complex after translocation. (*F*) Frames of traces during ongoing translation formed a peaked PRE-state distribution fit with a single Gaussian component ($n = 3664$ molecules).

FRET pair had two clear peaks that were fit with double Gaussian functions to provide the classical and hybrid FRET efficiencies for tRNA-L11 (0.73 ± 0.01 and 0.49 ± 0.02) and for tRNA-tRNA (0.68 ± 0.01 and 0.39 ± 0.01, Table 1, schemes A and B). Hidden Markov analysis of the fluctuating complexes, using HaMMy software (38), identified two states with essentially the same FRET values identified by fitting Gaussian components. Similar results were obtained for the stalled PRE-6, PRE-3, and PRE-2 complexes formed using labeling schemes D–G (Figs. S2–S6; Table 1). These classical and hybrid states had average dwell times in the range of 0.4–1.7 s (Table S1), measured by fitting exponential decays to their dwell time distributions (Fig. S7).

smFRET in PRE complexes formed during ongoing translation at 2 μM EF-G

tRNA-L11

In marked contrast to the results obtained with the stalled PRE-7 complex formed using V^7(Cy3)-L11(Cy5) in the absence of EF-G, the PRE-7 complex formed in the presence of EF-G during ongoing translation after six elongation cycles displayed a single, dominant, high-FRET efficiency centered at 0.65 ± 0.01 (Fig. 1 *F*; Table 1, scheme A) on binding of Val-tRNA^{Val}(Cy3) to the transient POST-6 complex (Fig. 1 *E*). This state was followed by a period with much lower FRET efficiency (<0.15), as expected for translocation of peptidyl-tRNA^{Val}(Cy3) to the P site. No FRET signal was observed when Phe-tRNA^{Phe}, cognate to codon 6, was omitted from the reaction mixture, demonstrating that the observed FRET events depended on translation from codon 1 to codon 7, which is cognate to Val-tRNA^{Val}(Cy3).

Importantly, contour plots derived from ongoing traces synchronized to the start (Fig. 3 *A*) or end (Fig. 3 *B*) of the high FRET events show a single, dominant state throughout their duration, with less than 6% of traces showing transitions to either the lower (0.49) or higher (0.73) efficiency characteristic of the stalled PRE-7 complex (Table S1). This low number of transitions implies a fluctuation rate slower than 0.03 s^{-1}, rather than the 0.6–2.3 s^{-1} that we observed in stalled ribosomes (Fig. 1 *B*), consistent with earlier results of ours showing that binding of EF-G suppresses classical-hybrid fluctuations established in stalled PRE complexes by at least 5–60 fold (21,39). In addition to this PRE-7 complex, measuring tRNA-L11 FRET during ongoing translation gave very similar results: almost no fluctuations for the PRE-6, PRE-3, and PRE-2

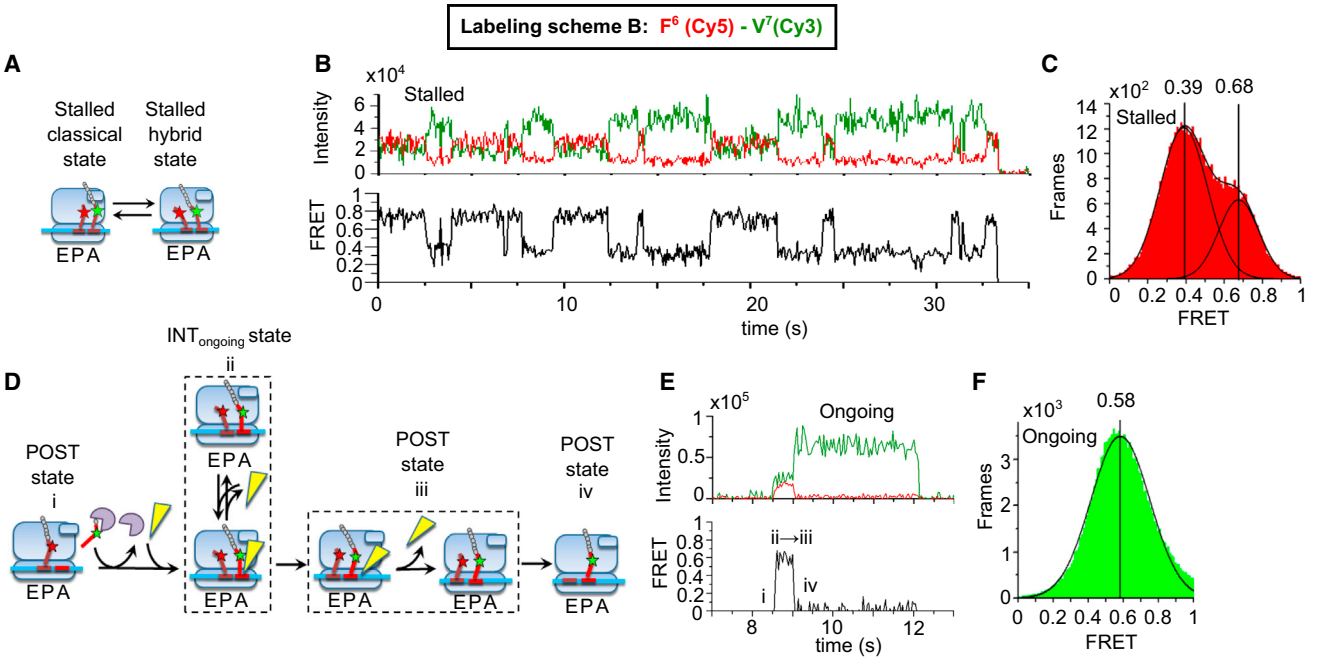

FIGURE 2 Stalled and ongoing tRNA-tRNA FRET measurements. Unlabeled ribosomes were programmed with mRNA-6,7 (Table 1) and Phe-tRNA^{Phe}(Cy5) at codon 6 underwent FRET with Val-tRNA^{Val}(Cy3) at codon 7. (*A*) Schematic of classical/hybrid equilibrium of a stalled ribosome. The green and red stars represent Cy3 fluorophore and Cy5 fluorophore, respectively. (*B*) Representative FRET recording. (*C*) Frames of fluctuating stalled traces formed a two-peaked distribution fit with a double Gaussian function ($n = 531$ molecules). (*D–F*) 2 μM EF-G was present during ongoing translation from codons 1–7. (*D*) Reaction scheme for ongoing translation. The yellow triangle represents EF-G; the purple disc represents EF-Tu. (*E*) A representative trace with the following FRET states: i) the POST state after the ribosome has translated through the fifth (Tyr) and sixth (Phe) codons, with peptidyl-tRNA^{Phe} residing in the P site; (ii, iii) INT$_{ongoing}$ and the initial POST state, which have similar FRET efficiencies (21); and iv) the POST state after dissociation of tRNA^{Phe}(Cy5) from the E-site. (*F*) Frames of traces during ongoing translation formed a peaked PRE state distribution fit with a single Gaussian component ($n = 2359$ molecules).

complexes earlier in elongation, with complexes formed using labeling schemes D–G (Figs. S2–S6; Table 1).

The nonfluctuating FRET state (which we term INT$_{ongoing}$) was also clearly shown in histograms formed from the average FRET efficiencies of FRET events in each trace during ongoing synthesis (Fig. S8, *A* and *B*, rather than from each movie frame as in Figs. 1, *C* and *F* and 2, *C* and *F*), which provides a complementary method of analyzing the data. Although histograms from frames (rather than event averages) better reflect the measurements' signal/noise ratios, the histograms of event averages reduce the frame-to-frame noise that might have caused an artefactual merger of FRET distributions arising from a wide bimodal population of PRE complexes. However, the peak centers remain the same, indicating that is not the case. In addition, negative cross-correlation of donor and acceptor intensities is a mark of fluctuating distance between tRNA and L11 in stalled PRE complexes. Lack of this negative cross-correlation in the PRE-7 complex formed during ongoing polypeptide synthesis provided additional evidence for the lack of distance fluctuations at the 35 ms camera timescale, and is further supported by time lag analysis of the decay of the stalled and ongoing cross-correlation signals (Fig. S8 *E*; Table S4).

The brief FRET events during ongoing translation (Fig. 1 *E*; Fig. S3 *E*, S4 *E*, S5 *E*, and S6 *E*) terminated upon translocation and dissociation of E-site tRNA. Duration histograms of the PRE states are shown in Fig. S7 and Table S2. In principle, the disappearance of FRET might also occur because of photobleaching of the Cy5 acceptor fluorophore. To check whether Cy5 photobleaching was a substantial contributor to the termination of the FRET events, a control experiment was performed alternating the excitation wavelength between 532 nm (to excite the Cy3 probes and measure FRET) and 640 nm to directly excite Cy5 (ALEX excitation, Fig. S1, *A–D*) (40). This procedure showed that the majority (>83%) of the FRET events at 2 μM EF-G terminated because of translocation rather than photobleaching (see Supporting Materials and Methods, *Photobleaching*). Because ALEX results in a two-fold decrease in time resolution of the experiment, subsequent data were collected without ALEX to obtain higher time resolution adequate for detecting fast fluctuations or transitions.

To distinguish whether the dominant single tRNA-L11 FRET state in ongoing translation (INT$_{ongoing}$) results from immediate binding of the TC to the previous POST state or from the presence of EF-G when the TC binds, we paused elongation at the POST-6 complex in the

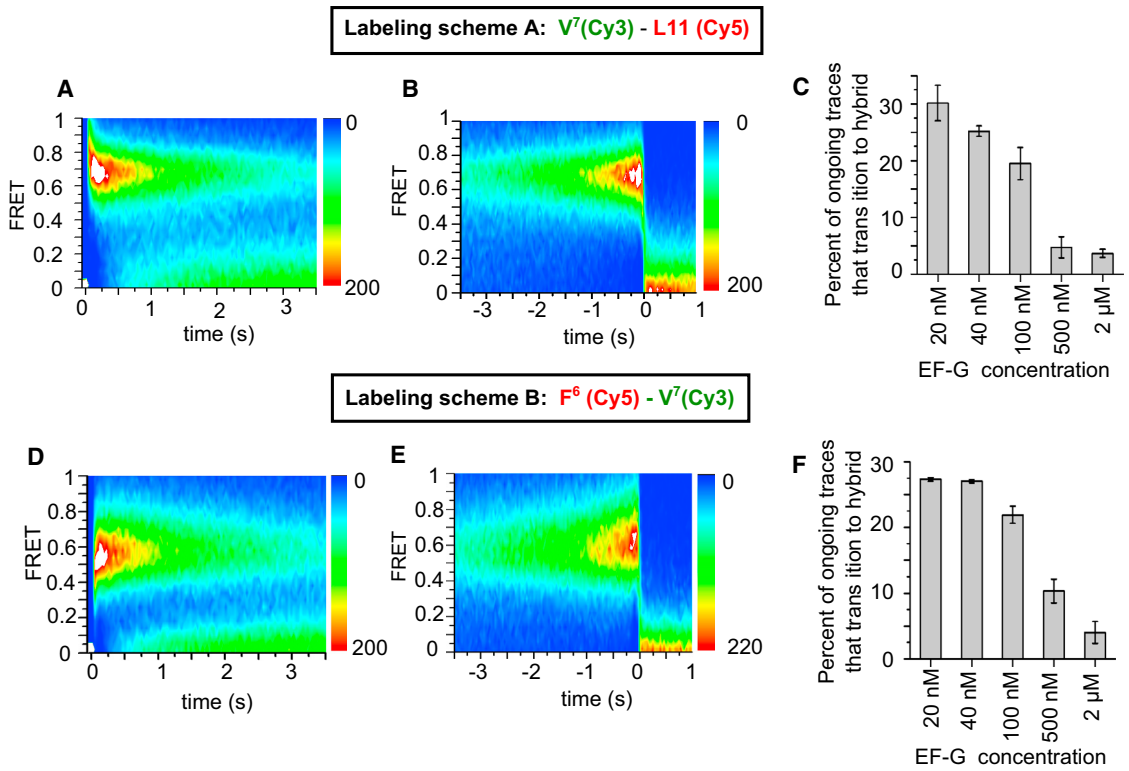

FIGURE 3 Dynamics of tRNA-L11 and tRNA-tRNA FRET. (*A–C*) L11(Cy5) ribosomes were programmed with mRNA-6,7 (Table 1) and underwent FRET with Val-tRNA^{Val}(Cy3). (*D–F*) Unlabeled ribosomes were programmed with mRNA-6,7 (Table 1), and Phe-tRNA^{Phe}(Cy5) at codon 6 underwent FRET with Val-tRNA^{Val}(Cy3) at codon 7, all in the presence of 2 μM EF-G during ongoing translation. FRET recordings were shifted in time to synchronize their beginnings ((*A* and *D*) presynchronized) or terminations ((*B* and *E*) postsynchronized) and overlaid to form contour plots. The color maps indicate the number of frames recorded at each FRET value and time. (*C* and *F*) Lowering EF-G concentration increased the percentage of fluctuating PRE complexes during ongoing translation; mean ± SE.

V^7(Cy3)-L11(Cy5) experiment by waiting 5 min before injecting Val-tRNA^{Val}(Cy3)·EF-Tu·GTP and EF-G·GTP together. We found the pause to have essentially no effect on the FRET results obtained, indicating that suppression of fluctuations and the intermediate FRET efficiency during ongoing translation do not arise as a consequence of the short lifetime of the POST-6 complex, but rather depend on EF-G being present when Val-TC is added to form PRE-7 (Fig. S1, *E–G*). Thus, when EF-G is present before PRE complex formation, the canonical classical-hybrid transitions found in stalled PRE complexes (Fig. 1, *A–C*) are almost completely absent (Table S3).

When FRET recordings were initiated before the addition of TC in the absence of EF-G, the initial PRE state was mainly classical and the partition between classical and hybrid emerged gradually during the next 5–15 s (Fig. S8, *I–K*). This contrasts strongly with the time course and distribution of FRET values in the presence of EF-G, which entered the state with FRET efficiency in between classical and hybrid values within 100 ms (Fig. 1; Fig. S3– S6).

tRNA-tRNA

The PRE-7 complex formed in the presence of EF-G during ongoing translation using F^6(Cy5)-V^7(Cy3), labeling scheme B, displays a single, dominant FRET efficiency (Fig. 2, *D–F*; Table 1, scheme B) that is in between the values found for the classical and hybrid tRNA positions, with minimal detectable fluctuations (Table S3), paralleling the tRNA-L11 results for INT$_{ongoing}$ reported above using V^7(Cy3)-L11(Cy5). As expected, FRET efficiency declines and becomes zero after translocation and dissociation of tRNA^{Phe} from the ribosome. That the tRNA-tRNA FRET efficiency in the transient POST-7 complex before tRNA^{Phe} dissociation is indistinguishable from the FRET efficiency of the corresponding PRE-7 complex is not surprising. We have previously shown that the tRNA-tRNA FRET efficiency in a POST complex formed on addition of EF-G to a stalled PRE complex has an intermediate value between those found for the classical and hybrid PRE complexes (21).

As mentioned, ALEX experiments ruled out a major component of Cy5 photobleaching in tRNA-L11 experiments. For tRNA-tRNA experiments, we could provide an additional safeguard against premature photobleaching by swapping the labeling positions. In labeling scheme C, F^6(Cy3)-V^7(Cy5) (Fig. S3, *D* and *E*), binding of tRNA^{Val}(Cy5) caused reduction of Cy3 fluorescence due to energy transfer, and both Cy3 and Cy5 fluorescence

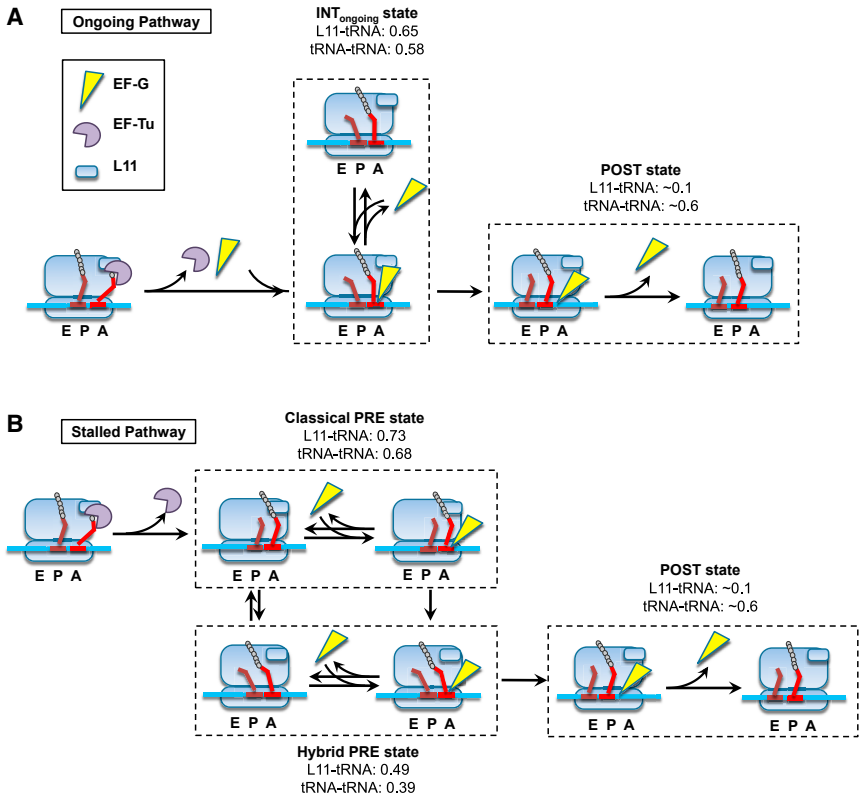

FIGURE 4 Schematics of divergent translocation pathways. In the ongoing translation pathway (*A*), newly formed PRE complexes occupy $INT_{ongoing}$ in the presence of EF-G, and quickly translocate. In the stalled pathway (*B*), relaxation of newly formed PRE complexes to a reversible distribution between stalled classical and hybrid tRNA positions in the absence of EF-G or at low EF-G concentrations. EF-G can interact with either state to promote translocation.

decreased after translocation and dissociation of the $tRNA^{Phe}$(Cy3). Photobleaching of the Cy5 after formation of the PRE state would have caused return of the high Cy3 fluorescence intensity, in contrast to its observed disappearance. Thus, the essentially identical results of FRET efficiency and virtually no fluctuations obtained using F^6(Cy5)-V^7(Cy3) (scheme B) and F^6(Cy3)-V^7(Cy5) (scheme C, Fig. S3; Table 1, scheme C) show that the stable PRE FRET state terminates upon translocation and dissociation of the E-site tRNA.

As discussed for tRNA-L11 FRET, event histograms for tRNA-tRNA FRET also exclude a merged bimodal population of classical and hybrid states during ongoing translation (Fig. S8, *C* and *D*), and cross-correlation analysis excludes fluctuations at or slower than the 35 ms frame rate (Fig. S8 *G*). The nonfluctuating $INT_{ongoing}$ conformation was also observed in experiments with a commonly used alternative buffer containing a lower (4.5 mM) Mg^{2+} concentration and polyamines (Supporting Materials and Methods (41)), thus it is not unique to the TAM_{15} buffer (Fig. S9).

PRE complex dwell times during ongoing translation

In the presence of 2 μM EF-G, all of the FRET pairs examined had dwell time distributions with both fast and slow phases, similar to what has been observed by others (24,42). Both phases had the same intermediate FRET value for all complexes studied. Dwell times for the fast phase (110–510 ms) and slow phase (1.2–2.5 s) (Fig. S7; Table S2), correspond to translocation rates of 2–9 s^{-1} and 0.4–0.8 s^{-1}, respectively, measured at 23°C. The fast-phase rates are reasonably consistent with in vivo rates of protein synthesis (12–21 s^{-1}) measured at 37°C (43), because the 14°C increase in temperature should result in $\geq$5-fold increase in translation rate, based on ensemble reconstituted, cell-free protein synthesis rates measured at 25°C (0.3 s^{-1} (44)) and 37°C (1.5 s^{-1} (45)). These rates are comparable to those previously reported for single-molecule reconstituted experiments: 0.57 s^{-1} at 30°C (35), 0.45 s^{-1} at room temperature (46), and 0.1−1 s^{-1} at room temperature (47).

smFRET in PRE-7 complexes formed during ongoing translation at decreasing EF-G

The experiments displayed in Figs. 1, 2, and S2–S6 demonstrate nearly complete absence of fluctuations or classical-hybrid transitions (Table S1) in the presence of 2 μM EF-G. The proportion of ribosomes exhibiting fluctuations increased as EF-G concentration was decreased to 20 nM (Fig. 3, *C* and *F*), which is attributable to delayed binding of EF-G to the PRE complex at low EF-G, thereby permitting temporary partitioning between the classical and hybrid positions. This interpretation is supported by the dynamics of those complexes that did fluctuate, which showed similar gradual establishment of classical-hybrid FRET values and fluctuations (Fig. S10). Although fluctuating PRE complexes at low EF-G concentrations translocated from either classical

or hybrid positions as previously observed (21–23), the proportion of translocation from the hybrid tRNA positions increased as EF-G concentration was lowered (Fig. S10).

DISCUSSION

Here we demonstrate that the presence of EF-G during ongoing polypeptide synthesis, even at a concentration (2 μM) well below that present in the bacterial cell [10–20 μM (48,49)], is sufficient to suppress fluctuations of tRNAs within PRE complexes during translocation. A single, dominant PRE-state intermediate during ongoing translation, termed $INT_{ongoing}$, is detected by either tRNA-L11 or tRNA-tRNA FRET (Table 1). We further show that such suppression is common within PRE-2 and PRE-3 complexes shortly after polypeptide synthesis is initiated, and within PRE-6 and PRE-7 complexes when the ribosome has moved out of the initial phase (50,51). tRNA-L11 and tRNA-tRNA FRET fluctuations appear as EF-G concentration is reduced below 500 nM, until between 20 and 40 nM EF-G, these fluctuations mimic those seen previously in stalled complexes (14,19,21,30,31,33) and here. This negative dependence of active site fluctuations on EF-G concentration provides strong evidence that such fluctuation will only occur if there is sufficient time between PRE complex formation on binding of the cognate TC and binding of EF-G to initiate translocation. At 2 μM, EF-G binds to the ribosome at a rate of $\sim$60–300 s^{-1} (52,53), suggesting that the onset of active site fluctuations in stalled PRE complexes requires times greater than 15 ms before EF-G binding.

A possible caveat to the conclusion that EF-G suppresses fluctuations and induces formation of a stable intermediate FRET state during translocation would be that bound EF-G strongly accelerates active site fluctuations so that, rather than occurring at rates of 0.5–2 s^{-1} (14,19,21,30,31,33), they occur at rates markedly faster than our experimental frame rate of 35 ms. If this were true, our FRET results (Table 1) during ongoing synthesis would correspond to two or more rapidly equilibrating states, rather than to a single state. Although we cannot formally rule out this possibility, the cross-correlation analysis of Fig. S8 indicates that such an acceleration would require vastly different dynamics than have ever been observed in a stalled ribosome.

In earlier studies, Sharma et al. (25,26) have shown that saturating EF-G accelerates the counterclockwise rotation of the 30S subunit with respect to the 50S subunit within the PRE complex by 5-fold, affording a rate constant of 12–14 s^{-1} under conditions (22°C, 15 mM Mg^{2+}) closely approximating our own. As mentioned, the putative tRNA-tRNA and tRNA-L11 fluctuations would have to proceed considerably more rapidly for us not to detect them. However, recent evidence strongly suggests that rotation of the 30S subunit with respect to the 50S subunit, or of the head region of the 30S subunit relative to the body, are both uncoupled from (and proceed more rapidly than) tRNA motions in either the stalled or translocating PRE complex (25,26). Because subunit rotations do not necessarily require fluctuations of the tRNA positions, they would be consistent with the stable intermediate tRNA conformation we observed.

This hypothesis raises the question of whether $INT_{ongoing}$ corresponds to a known or novel structure. The tRNA-tRNA FRET efficiency values reported in Table 1, 0.57 and 0.58, lead to apparent distances of $\sim$53 Å between the Cy3 and Cy5 dyes bound to the two tRNA D loops. These values are compatible with D-loop:D-loop tRNA-tRNA distances of 46–50 Å observed in three high-resolution structures of ribosomal complexes containing two tRNAs and bound EF-G before formation of the POST state (12,27,28). Those complexes were stabilized by the antibiotics neomycin and/or fusidic acid in conformations corresponding to neither the canonical classical or hybrid states formed in the absence of EF-G. An intermediate tRNA-tRNA FRET state was also formed on addition of EF-G to a stalled PRE complex in (24).

In contrast, the tRNA-L11 FRET efficiencies (0.63–0.69, Table 1) of $INT_{ongoing}$ correspond to distances of 49–51 Å between the Cy3 and Cy5 dyes bound to the peptidyl-tRNA D loop and position 87 of L11, which are inconsistent with distances of 77–81 Å estimated from the chimeric or hybrid state structures cited above (12,27,28). Instead, $INT_{ongoing}$ tRNA-L11 FRET efficiencies fall in between those found for the stalled classical and hybrid PRE complexes (but closer to the classical value). They are inconsistent with a putative translocation state identified in an L11-peptidyl-tRNA FRET study of Adio et al. (23), which has a FRET efficiency of 0.4, considerably lower than the FRET efficiencies determined for the stalled classical (0.8) and hybrid (0.6) complexes. In that study, for which translocation was initiated from a stalled PRE complex, no transient state was demonstrated on addition of native EF-G and GTP, but the 0.4 FRET state was demonstrated using a variety of protocols that stabilized translocation states, including the use of lower activity mutant variants of EF-G, the replacement of GTP by the nonhydrolyzable GTP analog GTPγS, and the addition of fusidic acid. This approach contrasts quite sharply with our use of native EF-G and GTP during ongoing translation in the absence of antibiotics. In addition, we labeled L11 at position 87, within the C-terminal domain, which interacts strongly with 23S ribosomal RNA (54,55), whereas Adio et al. labeled position 38 in the more flexible N-terminal domain that is held less tightly within the 50S structure, and may be freer to move during translocation.

Other than the continuous presence of EF-G during ongoing translation in the experiments presented here, it is unclear which of these further differences contribute to the discrepancy between our tRNA-L11 results and these other reports. The disparity between tRNA-L11 smFRET results summarized in Table 1 and the prior structural and smFRET results discussed above suggests that $INT_{ongoing}$ has tRNA

positions similar to the chimeric states, but a tRNA-L11 distance that has not been previously observed in structural or single molecule studies. We speculate that it most likely corresponds to an early stage of the translocation process that precedes the larger separation between L11 and peptidyl tRNA that has been seen in earlier work. On the other hand, given the known mobility of L11 within the ribosome structure (56), we cannot exclude the possibility that $INT_{ongoing}$ corresponds to a later stage of translocation involving a larger displacement of the C-terminal domain of L11 from the positions identified in previous reports.

Fig. 4 *A* is a scheme for ongoing protein synthesis that illustrates the main conclusions we draw from our results. During ongoing protein synthesis in the presence of ≥ 2 μM EF-G, cognate aminoacyl-tRNA binds transiently to an A/T site (Figs. S3, *D*, *E*, and *H*, and S6, *D*, *E*, and *H*) before moving directly to the $INT_{ongoing}$ state without detectable sampling of the canonical classical and hybrid states characteristic of stalled PRE complexes. It then translocates into the P site. EF-G is known to undergo rapid, reversible, nonproductive binding events before the final association that results in translocation (52,53,57), leading to the inclusion of the reversible dissociation and rebinding of EF-G to the PRE state in Fig. 4 *A*. The rapid phase of PRE-state dwell times, 110–510 ms (Table S2), is comparable to the average 200 ms residence time of EF-G on the ribosome during the final binding event that catalyzes translocation (57) at this temperature, indicating that the rapidly translocating ribosomes experience limited numbers of nonproductive interactions. Such interactions should be much more prevalent for the slowly translocating subpopulation having dwell times of 1.2–2.5 s. Despite this difference, rapidly and slowly translocating ribosomes had the same intermediate FRET value for each FRET pair, suggesting that the FRET value of $INT_{ongoing}$ results from EF-G interacting with the PRE complex during both rapid on-off events and the productive final interaction. This is in accord with earlier work demonstrating the effects of transient EF-G binding on ribosome dynamics (21).

We note that our study of the tRNA positions does not address large and small subunit rotations or fluctuations of their relative positions, which have been observed in many structural studies. As mentioned, the structural studies have required inhibitors or absence of EF-G to pause or stall translation. Chen et al. (22) have reported smFRET signals that monitored subunit rotations and fluctuations during ongoing translation at 200–500 nM EF-G, but these fluctuations were extremely slow, with dwell times greater than 10 s. Presumably, the very slow rotational fluctuations result from delayed EF-G binding or dramatic slowing by EF-G. Thus EF-G may also prevent the initiation of subunit rotational fluctuations. Given the high concentrations of EF-G in the cell, the translocation pathway of the tRNAs including $INT_{ongoing}$ (Fig. 4 *A*) is likely to be the dominant one, physiologically. However, an alternative pathway in which peptidyl-tRNA fluctuates between canonical classical and hybrid states in PRE complexes before translocation (Fig. 4 *B*) could be physiologically important when local EF-G concentration within the cell is atypically low.

SUPPORTING MATERIAL

Supporting Materials and Methods, ten figures, and four tables are available at http://www.biophysj.org/biophysj/supplemental/S0006-3495(17)30981-5.

AUTHOR CONTRIBUTIONS

R.M.J. performed experiments and analyzed data. R.M.J., C.C., B.S.C., and Y.E.G. designed research and wrote the article.

ACKNOWLEDGMENTS

This work was supported by National Institutes of Health grants GM080376 and GM118139 to B.S.C. and Y.E.G. C.C. was supported by an American Heart Association Postdoctoral Fellowship (12POST8910014). R.M.J. was supported by a National Institutes of Health Predoctoral Fellowship (F30AI114187).

REFERENCES

1. Cukras, A. R., D. R. Southworth, …, R. Green. 2003. Ribosomal proteins S12 and S13 function as control elements for translocation of the mRNA:tRNA complex. *Mol. Cell.* 12:321–328.
2. Fredrick, K., and H. F. Noller. 2003. Catalysis of ribosomal translocation by sparsomycin. *Science.* 300:1159–1162.
3. Gavrilova, L. P., O. E. Kostiashkina, …, A. S. Spirin. 1976. Factor-free ("non-enzymic") and factor-dependent systems of translation of polyuridylic acid by Escherichia coli ribosomes. *J. Mol. Biol.* 101:537–552.
4. Gavrilova, L. P., and A. S. Spirin. 1971. Stimulation of "non-enzymic" translocation in ribosomes by p-chloromercuribenzoate. *FEBS Lett.* 17:324–326.
5. Pestka, S. 1969. Studies on the formation of transfer ribonucleic acid-ribosome complexes. VI. Oligopeptide synthesis and translocation on ribosomes in the presence and absence of soluble transfer factors. *J. Biol. Chem.* 244:1533–1539.
6. Bretscher, M. S. 1968. Translocation in protein synthesis: a hybrid structure model. *Nature.* 218:675–677.
7. Moazed, D., and H. F. Noller. 1989. Intermediate states in the movement of transfer RNA in the ribosome. *Nature.* 342:142–148.
8. Blanchard, S. C., H. D. Kim, …, S. Chu. 2004. tRNA dynamics on the ribosome during translation. *Proc. Natl. Acad. Sci. USA.* 101:12893–12898.
9. Frank, J., and R. K. Agrawal. 2000. A ratchet-like inter-subunit reorganization of the ribosome during translocation. *Nature.* 406:318–322.
10. Dunkle, J. A., L. Wang, …, J. H. D. Cate. 2011. Structures of the bacterial ribosome in classical and hybrid states of tRNA binding. *Science.* 332:981–984.
11. Mohan, S., J. P. Donohue, and H. F. Noller. 2014. Molecular mechanics of 30S subunit head rotation. *Proc. Natl. Acad. Sci. USA.* 111:13325–13330.
12. Brilot, A. F., A. A. Korostelev, …, N. Grigorieff. 2013. Structure of the ribosome with elongation factor G trapped in the pretranslocation state. *Proc. Natl. Acad. Sci. USA.* 110:20994–20999.
13. Fischer, N., A. L. Konevega, …, H. Stark. 2010. Ribosome dynamics and tRNA movement by time-resolved electron cryomicroscopy. *Nature.* 466:329–333.

14. Fei, J., P. Kosuri, …, R. L. Gonzalez, Jr. 2008. Coupling of ribosomal L1 stalk and tRNA dynamics during translation elongation. *Mol. Cell.* 30:348–359.
15. Munro, J. B., R. B. Altman, …, S. C. Blanchard. 2007. Identification of two distinct hybrid state intermediates on the ribosome. *Mol. Cell.* 25:505–517.
16. Fei, J., J. E. Bronson, …, R. L. Gonzalez, Jr. 2009. Allosteric collaboration between elongation factor G and the ribosomal L1 stalk directs tRNA movements during translation. *Proc. Natl. Acad. Sci. USA.* 106:15702–15707.
17. Fei, J., A. C. Richard, …, R. L. Gonzalez, Jr. 2011. Transfer RNA-mediated regulation of ribosome dynamics during protein synthesis. *Nat. Struct. Mol. Biol.* 18:1043–1051.
18. Munro, J. B., R. B. Altman, …, S. C. Blanchard. 2010. A fast dynamic mode of the EF-G-bound ribosome. *EMBO J.* 29:770–781.
19. Cornish, P. V., D. N. Ermolenko, …, T. Ha. 2008. Spontaneous intersubunit rotation in single ribosomes. *Mol. Cell.* 30:578–588.
20. Cornish, P. V., D. N. Ermolenko, …, T. Ha. 2009. Following movement of the L1 stalk between three functional states in single ribosomes. *Proc. Natl. Acad. Sci. USA.* 106:2571–2576.
21. Chen, C., B. Stevens, …, B. S. Cooperman. 2011. Single-molecule fluorescence measurements of ribosomal translocation dynamics. *Mol. Cell.* 42:367–377.
22. Chen, J., A. Petrov, …, J. D. Puglisi. 2013. Coordinated conformational and compositional dynamics drive ribosome translocation. *Nat. Struct. Mol. Biol.* 20:718–727.
23. Adio, S., T. Senyushkina, …, M. V. Rodnina. 2015. Fluctuations between multiple EF-G-induced chimeric tRNA states during translocation on the ribosome. *Nat. Commun.* 6:7442.
24. Wasserman, M. R., J. L. Alejo, …, S. C. Blanchard. 2016. Multiperspective smFRET reveals rate-determining late intermediates of ribosomal translocation. *Nat. Struct. Mol. Biol.* 23:333–341.
25. Belardinelli, R., H. Sharma, …, M. V. Rodnina. 2016. Choreography of molecular movements during ribosome progression along mRNA. *Nat. Struct. Mol. Biol.* 23:342–348.
26. Sharma, H., S. Adio, …, M. V. Rodnina. 2016. Kinetics of spontaneous and EF-G-accelerated rotation of ribosomal subunits. *Cell Reports.* 16:2187–2196.
27. Zhou, J., L. Lancaster, …, H. F. Noller. 2014. How the ribosome hands the A-site tRNA to the P site during EF-G-catalyzed translocation. *Science.* 345:1188–1191.
28. Ramrath, D. J. F., L. Lancaster, …, C. M. T. Spahn. 2013. Visualization of two transfer RNAs trapped in transit during elongation factor G-mediated translocation. *Proc. Natl. Acad. Sci. USA.* 110:20964–20969.
29. Frank, J., and R. L. Gonzalez, Jr. 2010. Structure and dynamics of a processive Brownian motor: the translating ribosome. *Annu. Rev. Biochem.* 79:381–412.
30. Munro, J. B., R. B. Altman, …, S. C. Blanchard. 2010. Spontaneous formation of the unlocked state of the ribosome is a multistep process. *Proc. Natl. Acad. Sci. USA.* 107:709–714.
31. Kim, H. D., J. D. Puglisi, and S. Chu. 2007. Fluctuations of transfer RNAs between classical and hybrid states. *Biophys. J.* 93:3575–3582.
32. Munro, J. B., R. B. Altman, …, S. C. Blanchard. 2007. Identification of two distinct hybrid state intermediates on the ribosome. *Mol. Cell.* 25:505–517.
33. Wang, B., J. Ho, …, Q. Lin. 2011. A microfluidic approach for investigating the temperature dependence of biomolecular activity with single-molecule resolution. *Lab Chip.* 11:274–281.
34. Ning, W., J. Fei, and R. L. Gonzalez, Jr. 2014. The ribosome uses cooperative conformational changes to maximize and regulate the efficiency of translation. *Proc. Natl. Acad. Sci. USA.* 111:12073–12078.
35. Rosenblum, G., C. Chen, …, B. S. Cooperman. 2013. Quantifying elongation rhythm during full-length protein synthesis. *J. Am. Chem. Soc.* 135:11322–11329.
36. Kaur, J., M. Raj, and B. S. Cooperman. 2011. Fluorescent labeling of tRNA dihydrouridine residues: mechanism and distribution. *RNA.* 17:1393–1400.
37. Roy, R., S. Hohng, and T. Ha. 2008. A practical guide to single-molecule FRET. *Nat. Methods.* 5:507–516.
38. McKinney, S. A., C. Joo, and T. Ha. 2006. Analysis of single-molecule FRET trajectories using hidden markov modeling. *Biophys. J.* 19:1941–1951.
39. Chen, C., M. J. Greenberg, …, H. Shuman. 2012. Kinetic schemes for post-synchronized single molecule dynamics. *Biophys. J.* 102:L23–L25.
40. Kapanidis, A. N., T. A. Laurence, …, S. Weiss. 2005. Alternating-laser excitation of single molecules. *Acc. Chem. Res.* 38:523–533.
41. Dinos, G., D. L. Kalpaxis, …, K. H. Nierhaus. 2005. Deacylated tRNA is released from the E site upon A site occupation but before GTP is hydrolyzed by EF-Tu. *Nucleic Acids Res.* 33:5291–5296.
42. Wang, L., A. Pulk, …, S. C. Blanchard. 2012. Allosteric control of the ribosome by small-molecule antibiotics. *Nat. Struct. Mol. Biol.* 19:957–963.
43. Young, R., and H. Bremer. 1976. Polypeptide-chain-elongation rate in Escherichia coli B/r as a function of growth rate. *Biochem. J.* 160:185–194.
44. Takahashi, S., K. Tsuji, …, Y. Okahata. 2012. Traveling Time of a translating ribosome along messenger RNA monitored directly on a quartz crystal microbalance. *J. Am. Chem. Soc.* 134:6793–6800.
45. Underwood, K. A., J. R. Swartz, and J. D. Puglisi. 2005. Quantitative polysome analysis identifies limitations in bacterial cell-free protein synthesis. *Biotechnol. Bioeng.* 91:425–435.
46. Wen, J.-D., L. Lancaster, …, I. Tinoco. 2008. Following translation by single ribosomes one codon at a time. *Nature.* 452:598–603.
47. Uemura, S., C. E. Aitken, …, J. D. Puglisi. 2010. Real-time tRNA transit on single translating ribosomes at codon resolution. *Nature.* 464:1012–1017.
48. Kurland, C. G., D. Hughes, and H. Ehrenberg. 1995. Escherichia coli and Salmonella typhimurium: Cellular and Molecular Biology. American Society for Microbiology, Washington DC.
49. Munishkin, A., and I. G. Wool. 1997. The ribosome-in-pieces: binding of elongation factor EF-G to oligoribonucleotides that mimic the sarcin/ricin and thiostrepton domains of 23S ribosomal RNA. *Proc. Natl. Acad. Sci. USA.* 94:12280–12284.
50. Tenson, T., and V. Hauryliuk. 2009. Does the ribosome have initiation and elongation modes of translation? *Mol. Microbiol.* 72:1310–1315.
51. Chen, C., B. Stevens, …, Y. E. Goldman. 2011. Allosteric vs spontaneous exit-site (E-site) tRNA dissociation early in protein synthesis. *Proc. Natl. Acad. Sci. USA.* 108:16980–16985.
52. Katunin, V. I., A. Savelsbergh, …, W. Wintermeyer. 2002. Coupling of GTP hydrolysis by elongation factor G to translocation and factor recycling on the ribosome. *Biochemistry.* 41:12806–12812.
53. Seo, H.-S., M. Kiel, …, B. S. Cooperman. 2004. Kinetics and thermodynamics of RRF, EF-G, and thiostrepton interaction on the Escherichia coli ribosome. *Biochemistry.* 43:12728–12740.
54. Wimberly, B. T., R. Guymon, …, V. Ramakrishnan. 1999. A detailed view of a ribosomal active site: the structure of the L11-RNA complex. *Cell.* 97:491–502.
55. Conn, G. L., D. E. Draper, …, A. G. Gittis. 1999. Crystal structure of a conserved ribosomal protein-RNA complex. *Science.* 284:1171–1174.
56. Kavran, J. M., and T. A. Steitz. 2007. Structure of the base of the L7/L12 stalk of the Haloarcula marismortui large ribosomal subunit: analysis of L11 movements. *J. Mol. Biol.* 371:1047–1059.
57. Chen, C., X. Cui, …, Y. E. Goldman. 2016. Elongation factor G initiates translocation through a power stroke. *Proc. Natl. Acad. Sci. USA.* 113:7515–7520.

Biophysical Journal, Volume *113*

Supplemental Information

tRNA Fluctuations Observed on Stalled Ribosomes Are Suppressed during Ongoing Protein Synthesis

Ryan M. Jamiolkowski, Chunlai Chen, Barry S. Cooperman, and Yale E. Goldman

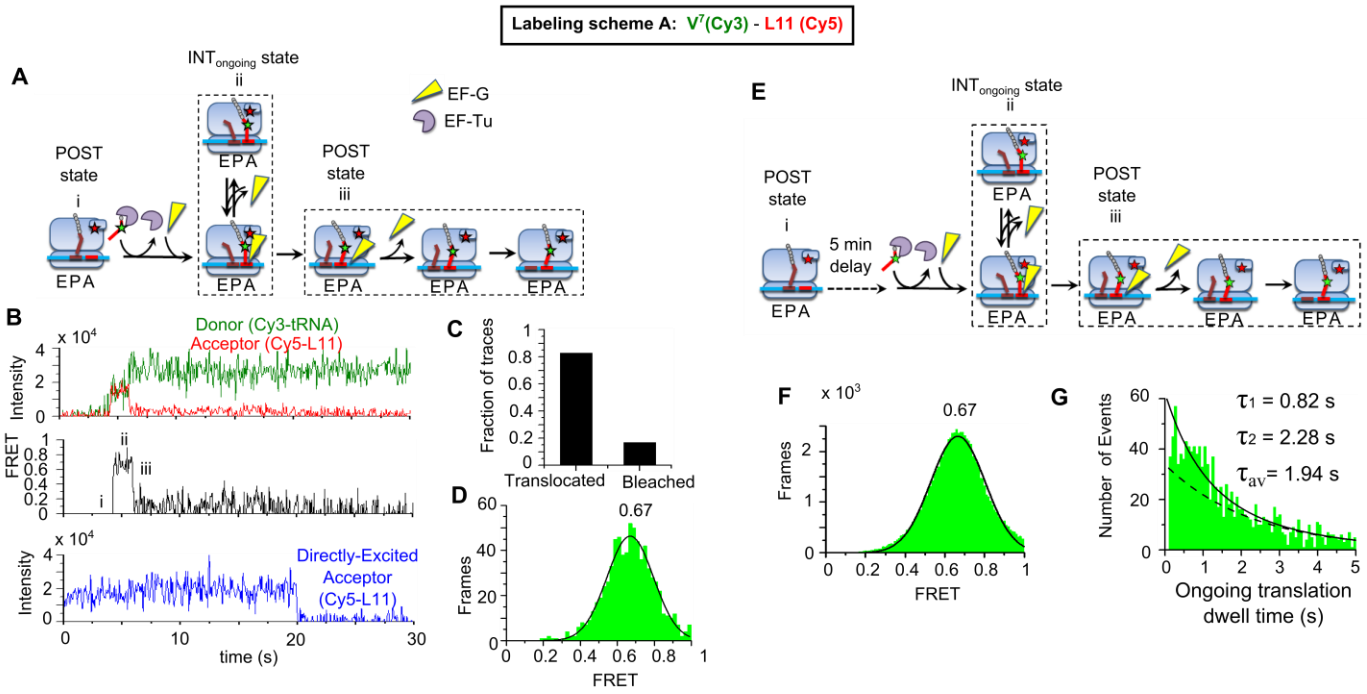

Figure S1. Control experiments for tRNA-L11 smFRET measurements. L11(Cy5) ribosomes were programmed with mRNA-6,7 (Table 1) and underwent FRET with Val-tRNA^{Val}(Cy3). **(A)** Reaction scheme for ongoing translation, **(B)** a representative trace using alternating laser excitation (ALEX) with the following FRET states: **(i)** the POST state after the ribosome has translated from the 1st through the 5th (Tyr) and 6th (Phe) codons, and peptidyl-tRNA^{Phe} residing in the P-site; **(ii)** INT$_{ongoing}$; and **(iii)** the POST complex following translocation. **(C)** Using ALEX, 83% of the traces were shown to translocate before photobleaching, and **(D)** the FRET efficiencies from the frames of non-bleached traces formed a distribution with approximately the same peak center as observed without ALEX**.** **(E)** The same L11(Cy5) ribosomes programmed with mRNA-6,7 were delayed by 5 minutes after the formation of a POST state with peptidyl-tRNA^{Phe} residing in the P-site before addition of Val-tRNA^{Val}(Cy3) and 2 µM EF-G**.** The detected FRET during subsequent INT$_{ongoing}$ occupancy formed a distribution with approximately the same peak center **(F)** and dwell times **(G)** as observed without the POST delay.

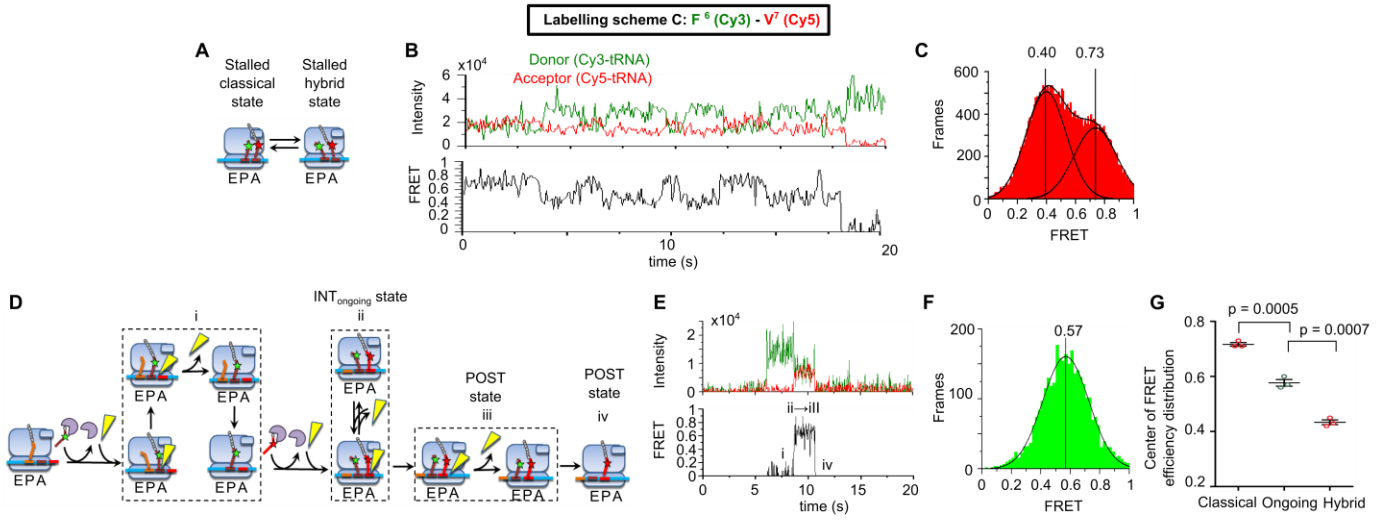

Figure S2. tRNA-tRNA FRET with labels swapped. Unlabeled ribosomes programmed with mRNA-6,7 (Table 1) and Phe-tRNA^{Phe}(Cy3) at codon 6 underwent FRET with Val-tRNA^{Val}(Cy5) at codon 7. **(A)** Schematic of classical/hybrid equilibrium of a stalled ribosome with **(B)** representative FRET recording**. (C)** Frames of fluctuating stalled traces formed a two-peaked distribution fitted by a double Gaussian function (n = 497 molecules). For **(D-F),** EF-G was present at 2 µM during ongoing translation. **(D)** Reaction scheme for ongoing translation, **(E**) a representative trace with the following FRET states: **(i)** an entire translocation cycle with Phe-tRNA^{Phe}(Cy3) entering the A-site and translocating to the P-site, resulting in a POST state after the ribosome has translated from the 1st through the 5th (Tyr) and 6th (Phe) codons; **(ii, iii)** INT$_{ongoing}$ and the initial POST state, which have similar FRET efficiencies (Chen et al., 2011); and **(iv)** the POST state following dissociation of tRNA^{Phe}(Cy3) from the E-site. **(F)** Frames of traces during ongoing translation formed a peaked distribution fitted with a single Gaussian component (INT$_{ongoing}$, n = 200 molecules). **(G)** FRET distribution peak centers for ongoing translation were statistically different from the stalled classical and hybrid peaks over multiple replicate experiments (means ± SEM)**.**

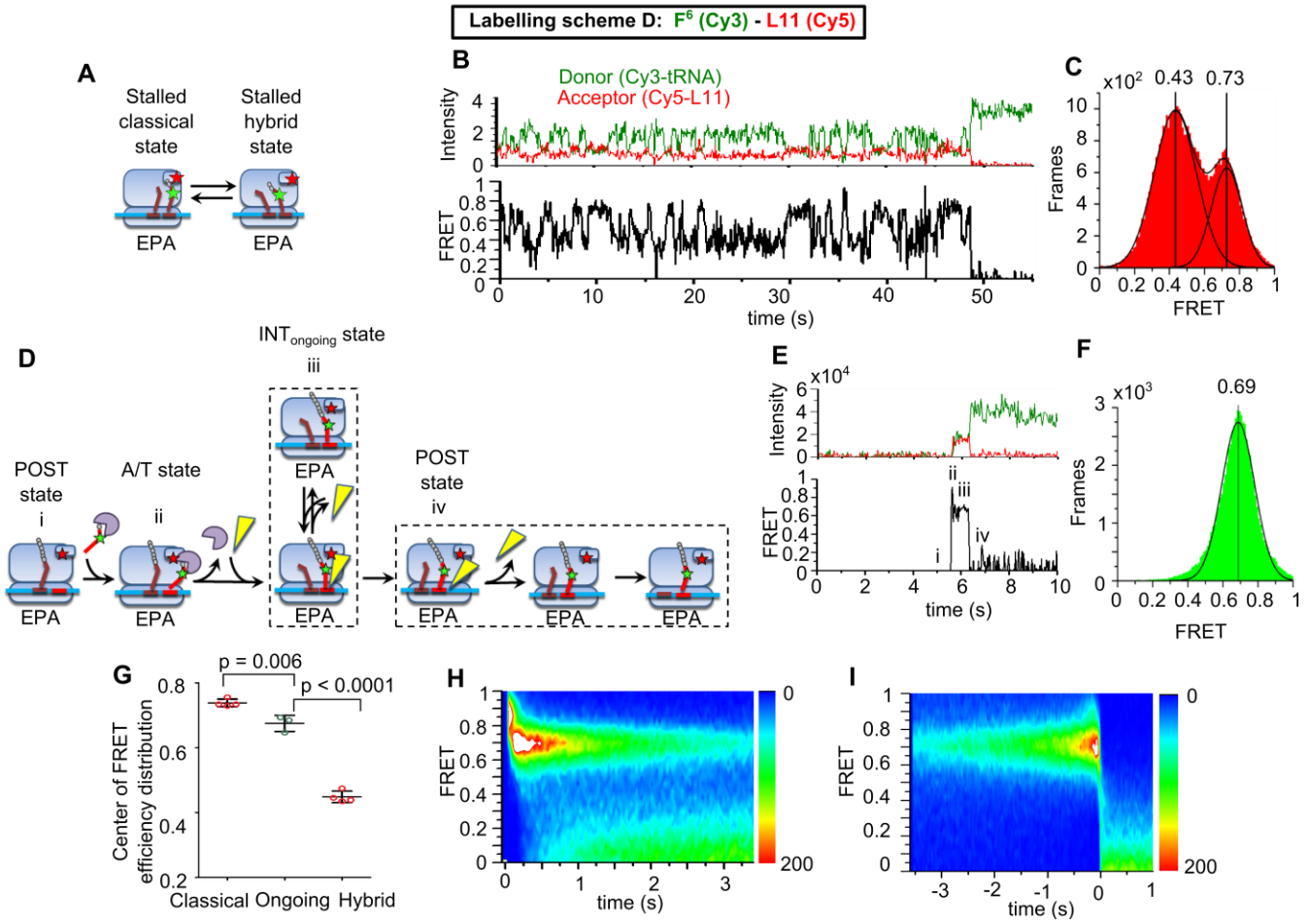

Figure S3. tRNA^{Phe}-L11 FRET in PRE-6. L11(Cy5) ribosomes were programmed with mRNA-6,7 and underwent FRET with Phe-tRNA^{Phe}(Cy3). **(A)** Reaction scheme of classical/hybrid equilibrium of stalled ribosomes. **(B)** Representative stalled FRET recording. **(C)** Frames of fluctuating stalled traces formed a two-peaked FRET distribution fitted with a double Gaussian function (**C**, n = 451 molecules,). For **(D-I),** EF-G was present at 2 µM during ongoing translation. **(D)** Reaction scheme for ongoing translation. **(E**) Representative trace with the following FRET states: **(i)** the POST state with peptidyl-tRNA^{Tyr} at the 5th codon residing in the P-site; **(ii)** the very high FRET A/T state during Phe-tRNA^{Phe} delivery but before full accommodation (seen in ~20% of traces) as reported by others using Phe-tRNA^{Phe}-L11 FRET (Geggier et al., 2010). A similar state was seen in a small minority (<5%) of Val-tRNA^{Val}- L11 FRET traces during ongoing translation, but was much less prominent; **(iii)** INT$_{ongoing}$; and **(iv)** the POST complex following translocation. **(F)** Frames of traces during ongoing translation formed a peaked PRE state distribution fitted with a single Gaussian component (n = 1423 molecules). **(G)** FRET distribution peak centers for ongoing translation were statistically different from the stalled classical and hybrid peaks over multiple replicate experiments (means ± SEM). FRET recordings were shifted in time to synchronize their beginnings (**H**, pre-synchronized) or terminations (**I,** post-synchronized) and overlaid to form contour plots. The color maps indicate number of frames recorded at each FRET value and time.

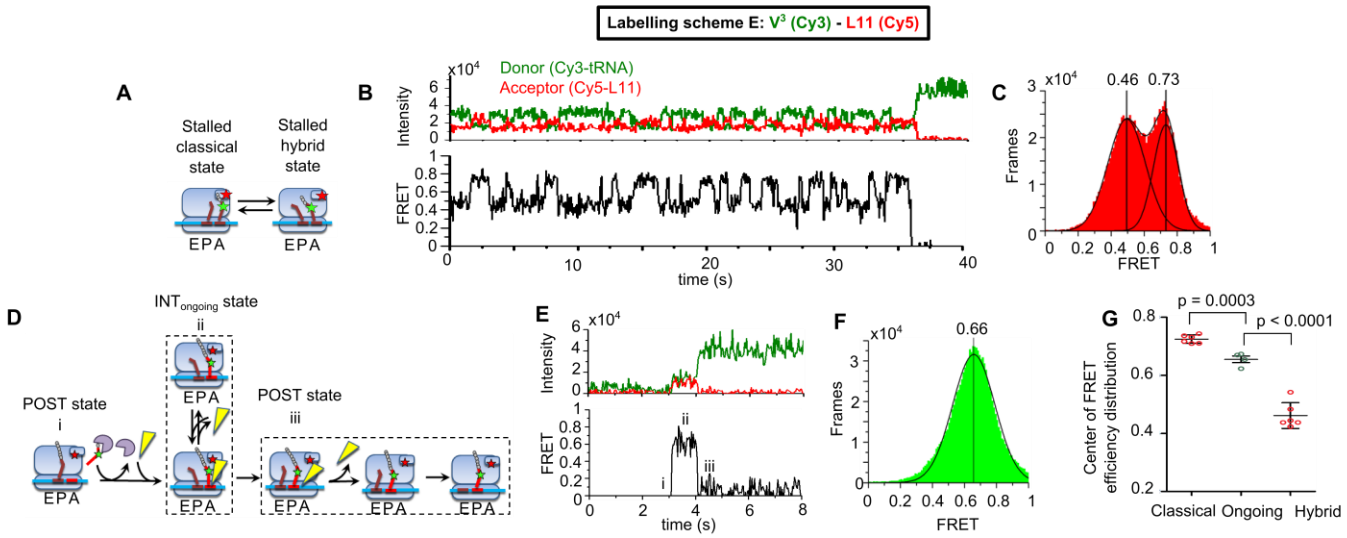

Figure S4: **tRNA^{Val}-L11 FRET early in translation (in PRE-3).** L11(Cy5) ribosomes were programmed with mRNA-2,3 (Table 1) and underwent FRET with Val-tRNA^{Val} (Cy5). **(A)** Schematic of classic/hybrid equilibrium of stalled ribosomes with **(B)** a representative FRET recording**. (C)** Frames of fluctuating stalled traces formed a two-peaked distribution fitted with a double Gaussian function (n = 541 molecules). For **(D-F)** EF-G was present at 2 µM during ongoing translation. **(D)** Reaction scheme for ongoing translation, **(E)** representative FRET recording with the following FRET states: **(i)** the POST state after the ribosome has translated through the 1st (fMet) and 2nd (Phe) codons, with peptidyl-tRNA^{Phe} residing in the P-site; **(ii)** INT$_{ongoing}$; and **(iii)** the POST complex following translocation. **(F)** Frames of traces during ongoing translation formed a peaked PRE state distribution fitted with a single Gaussian component (INT$_{ongoing}$, n = 2157 molecules). **(G)** FRET distribution peak centers for ongoing translation were statistically different from the stalled classical and hybrid peaks over multiple replicate experiments (means ± SEM)**.**

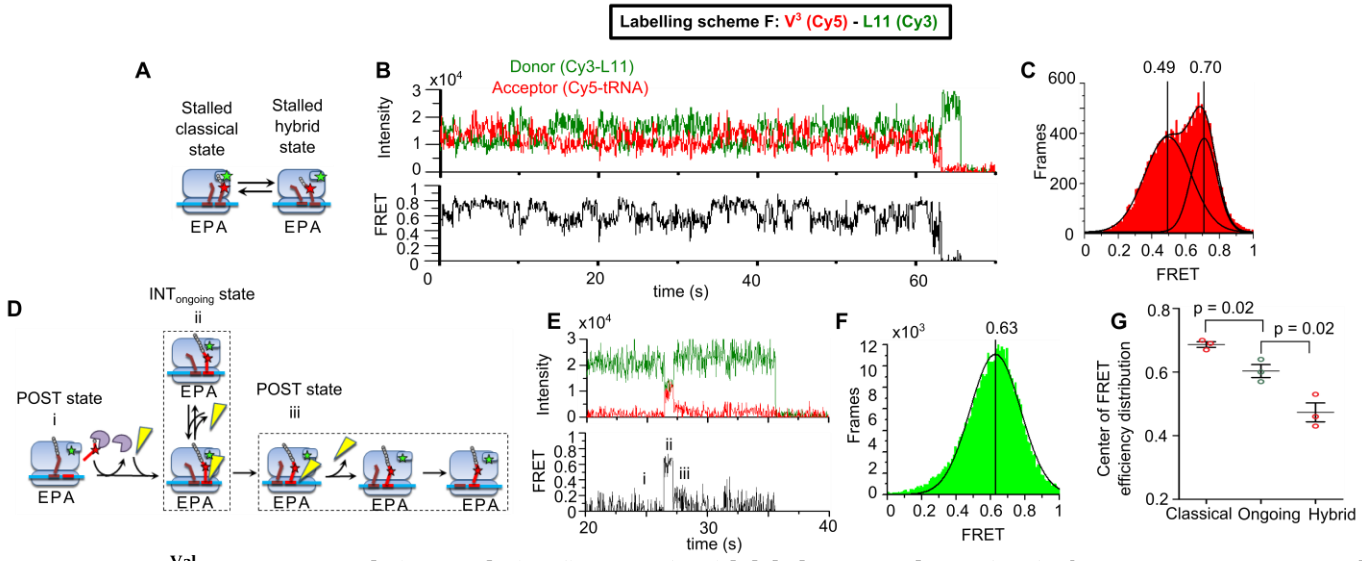

Figure S5. **tRNA^{Val}-L11 FRET early in translation (in PRE-3), with labels swapped.** L11(Cy3) ribosomes were programmed with mRNA-2,3 (Table 1) and underwent FRET with Val-tRNA^{Val}(Cy5). **(A)** Schematic of classic/hybrid equilibrium of stalled ribosomes with **(B)** a representative FRET recording**. (C)** Frames of fluctuating stalled traces formed a two-peaked distribution fitted with a double Gaussian function (n = 139 molecules). For **(D-F),** EF-G was present at 2 µM during ongoing translation. **(D)** Reaction scheme for ongoing translation, **(E)** representative FRET recording with the following FRET states: **(i)** the POST state after the ribosome has translated through the 1st (fMet) and 2nd (Phe) codons, with peptidyl-tRNA^{Phe} residing in the P-site; **(ii)** INT$_{ongoing}$; and **(iii)** the POST complex following translocation. **(F)** Frames of traces during ongoing translation formed a peaked PRE state distribution fitted with a single Gaussian component (n = 319 molecules). **(G)** FRET distribution peak centers for ongoing translation were statistically different from the stalled classical and hybrid peaks over multiple replicate experiments (means ± SEM)**.**

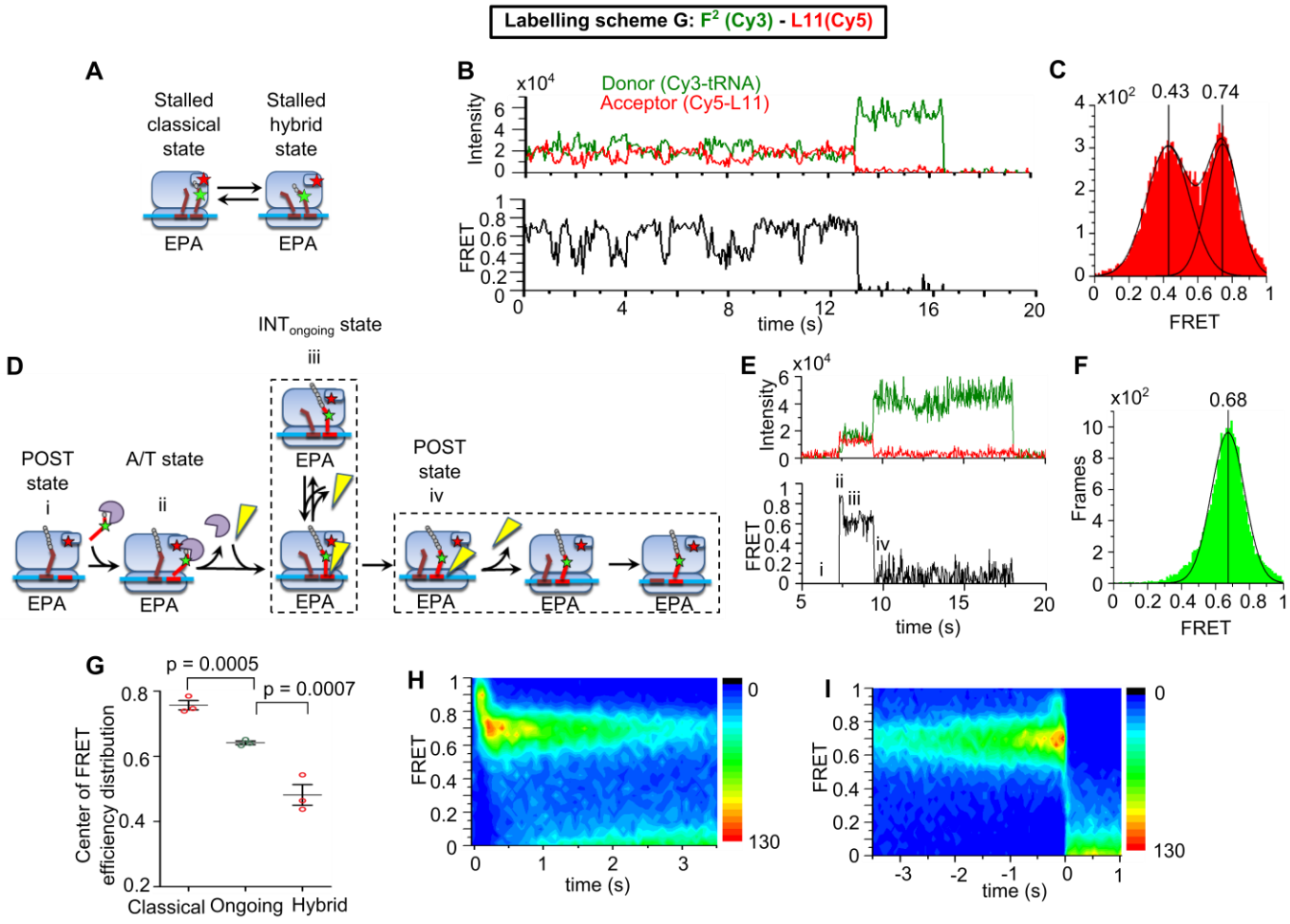

Figure S6. tRNA^{Phe}-L11 FRET very early in translation (in PRE-2). L11(Cy5) ribosomes were programmed with mRNA-2,3 and underwent FRET with Phe-tRNA^{Phe}(Cy3). **(A)** Reaction scheme of classical/hybrid equilibrium of stalled ribosomes. **(B)** Representative stalled FRET recording. **(C)** Frames of fluctuating stalled traces formed a two-peaked distribution fitted with a double Gaussian function (n = 237 molecules). For **(D-I),** EF-G was present at 2 µM during ongoing translation. **(D)** Reaction scheme for ongoing translation. **(E)** Representative trace with the following FRET states: **(i)** fMet-tRNA^{fMet} at the 1st codon residing in the P-site; **(ii)** the very high FRET A/T state during Phe-tRNA^{Phe} delivery but before full accommodation (seen in ~20% of traces) and reported by others using Phe-tRNA^{Phe}- L11 FRET (Geggier et al., 2010). **(iii)** INT$_{ongoing}$; and **(iv)** the POST complex following translocation. **(F)** Frames of traces during ongoing translation formed a peaked PRE state distribution fitted with a single Gaussian component (n = 434 molecules). **(G)** FRET distribution peak centers for ongoing translation were statistically different from the stalled classical and hybrid peaks over multiple replicate experiments (means ± SEM). FRET recordings were shifted in time to synchronize their beginnings (**H**, pre-synchronized) or terminations (**I**, post-synchronized) and overlaid to form contour plots. The color maps indicate number of frames recorded at each FRET value and time.

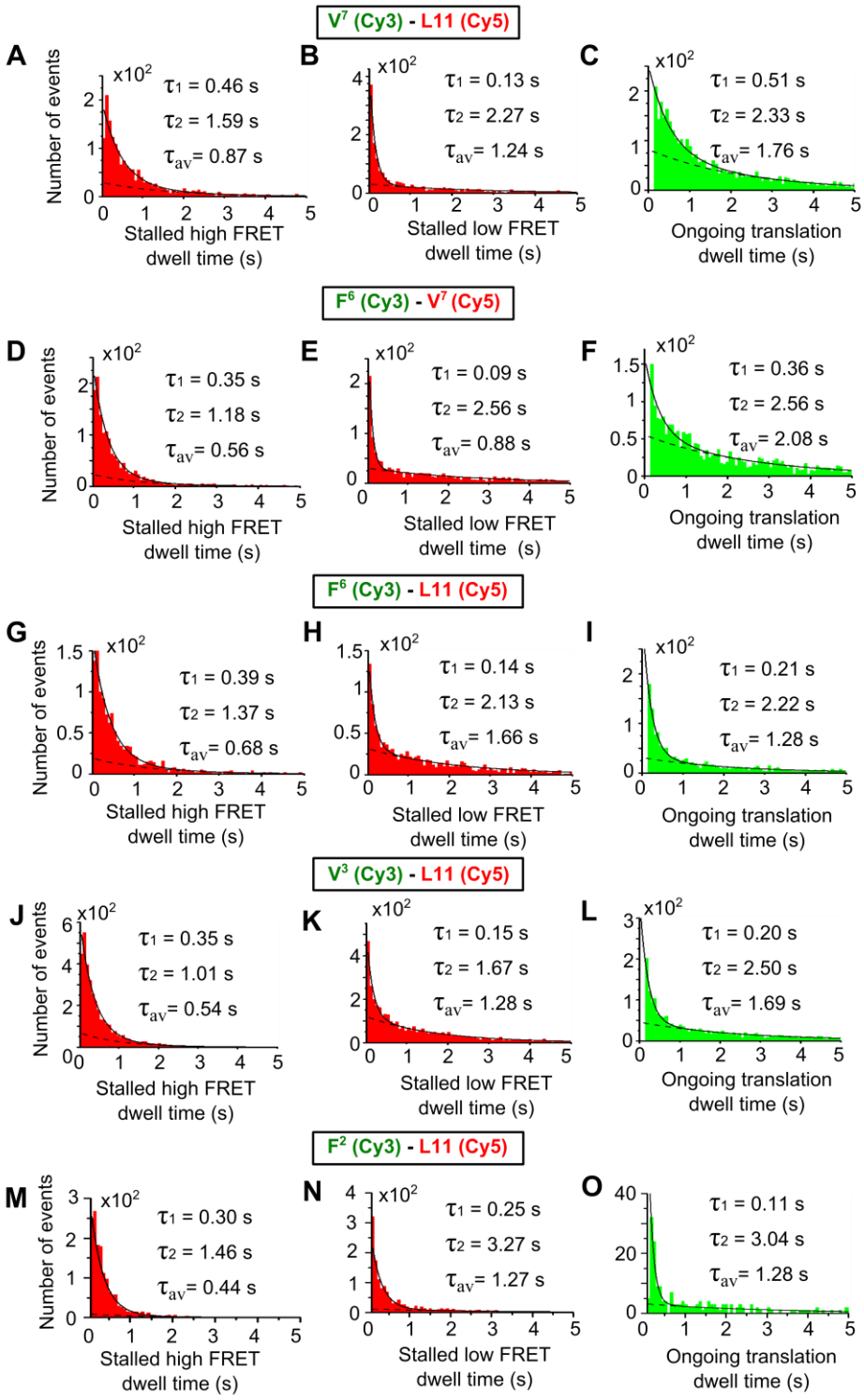

Figure S7. **Dwell times for the stalled classical and hybrid tRNA positions, and the ongoing intermediate state at 2 μM EF-G**. Double exponential fitting gave fast and slow phases for the lifetimes of each state, and weighted average durations, τ_{av}, according to Eq. S5, in Supplemental Methods.

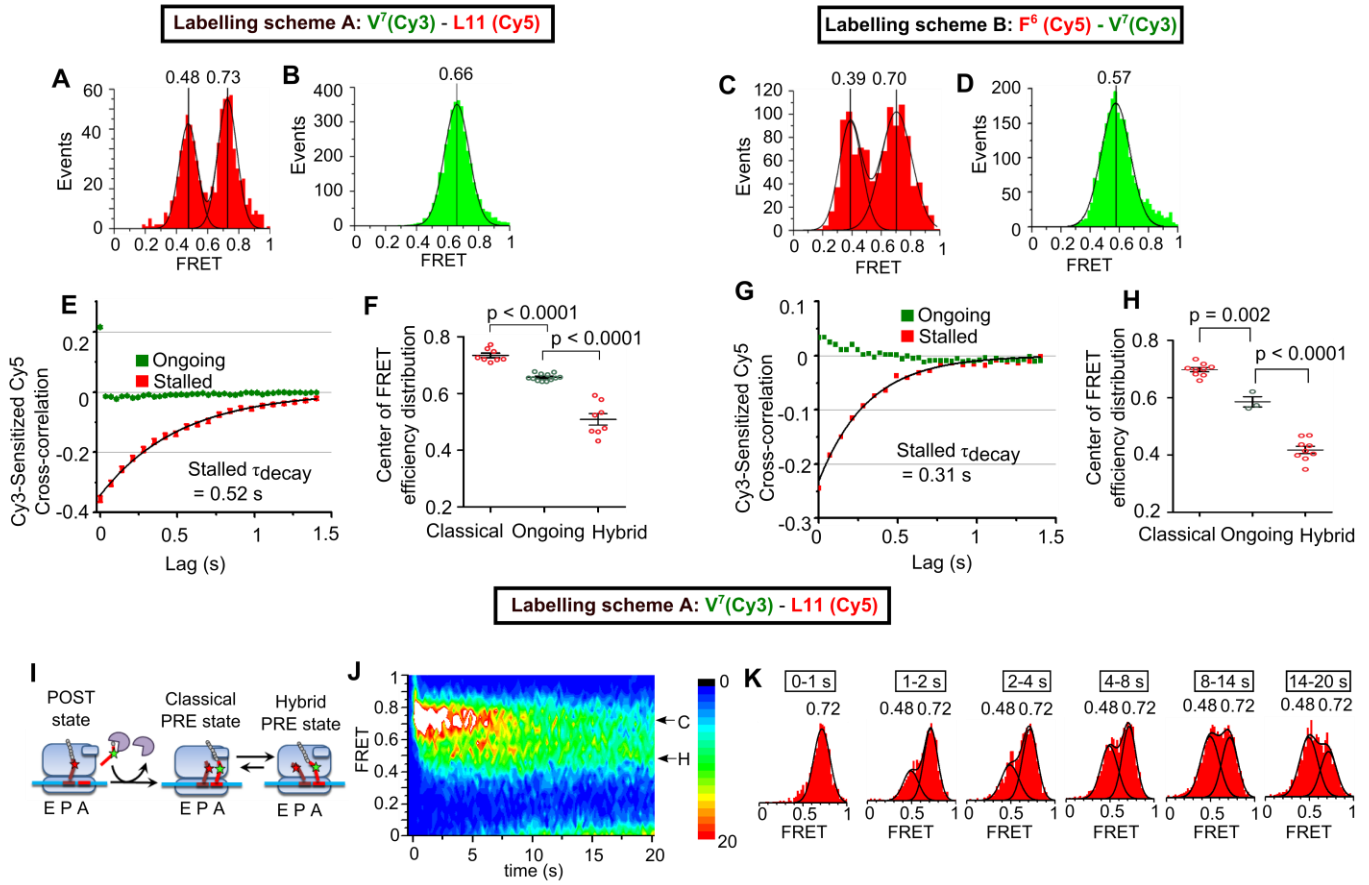

Figure S8. Event histograms, cross-correlation dynamics and temporal development of hybrid-classical partition. For both V^7(Cy3)-L11(Cy5) and F^6(Cy3)-V^7(Cy5) experiments, the average FRET efficiencies of each high or low FRET occupancy event from the stalled traces formed two-peaked event distributions **(A,C)**, while the average FRET efficiencies of each ongoing trace formed a single-peaked event distribution **(B, D)**. These event distributions are more narrow than the temporal histograms, from individual frames, presented in the main text, because frame-to-frame noise (due to photon counting, camera amplification and laser noise) are averaged out in these pre-averaged (event) histograms. The peaks of their distributions are the same as the temporal histograms, demonstrating that those positions are not biased by the frame-to-frame noise. **(E,G)** Cross-correlation of donor and acceptor intensities (Eq. S7) as a function of temporal lag for stalled ribosomes (red) and ribosomes during ongoing translation (green); SEM <0.01, too small to be visible on the graph. **(F,H)** FRET distribution peak centers for ongoing translation were statistically different from the stalled classical and hybrid peaks over multiple replicate experiments (means ± SEM). **(I-K)** Formation of the PRE complex in the absence of EF-G was observed by injecting Val-$tRNA^{Val}$(Cy3) ternary complex without EF-G into flow chambers containing stalled L11- POST-translocation ribosomes with peptidyl-Phe-$tRNA^{Phe}$ in their P-sites and vacant A-sites**.** The subsequent FRET recordings lasting from tRNA binding until photobleaching, and were used to form a pre-synchronized 2D contour plot **(J)** and histograms of cross-sections through the contour plot at indicated times **(K).** The tRNA-L11 FRET pair initially exhibits high (classical) FRET efficiency before partitioning into a classical-hybrid equilibrium without adopting the intermediate state seen during ongoing translation at 2 μM EF-G (n =192 molecules).

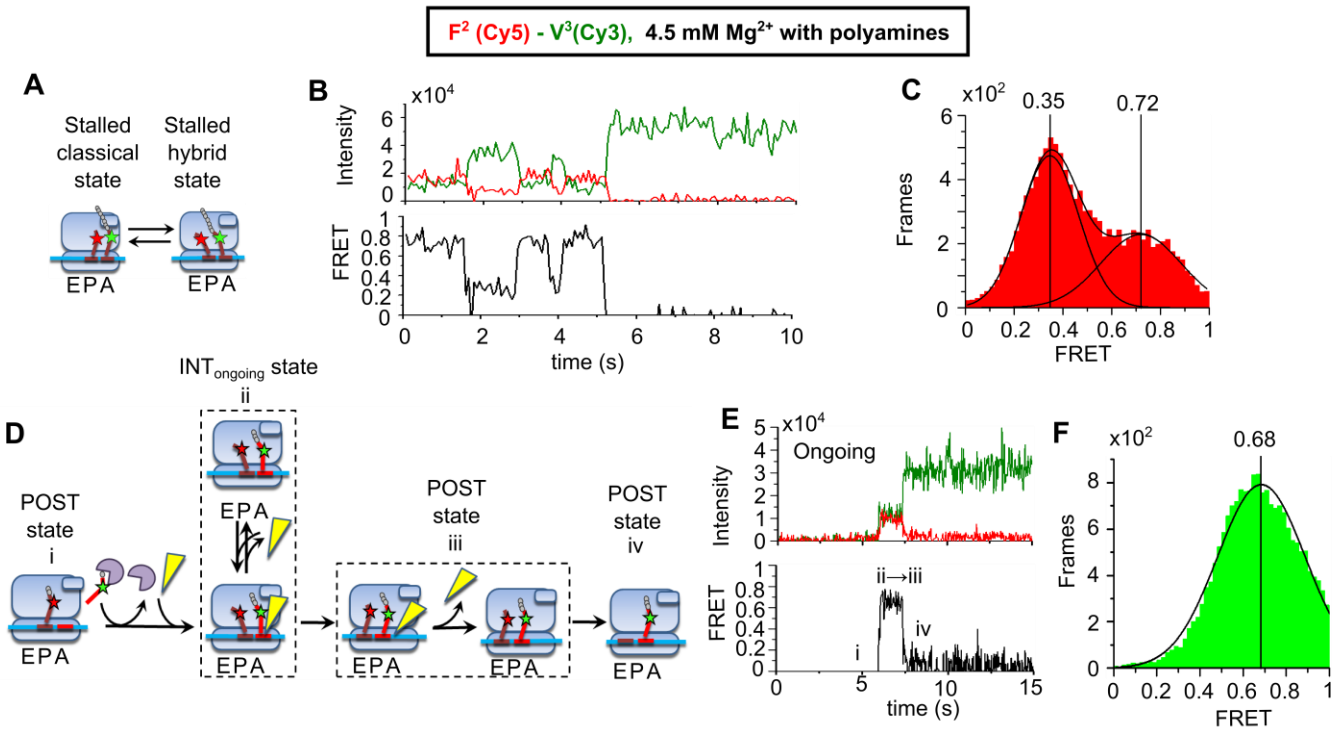

Figure S9. Stalled and ongoing tRNA-tRNA FRET measurements at 4.5 mM Mg^{2+}. Experiments were conducted in buffer consisting of: 50 mM HEPES-KOH (pH 7.3), 4.5 mM $MgAc_2$, 4 mM 2-mercaptoethanol, 150 mM NH_4Ac, 0.05 mM spermine, 2 mM spermidine. Unlabeled ribosomes were programmed with mRNA-2,3 (Table 1) and Phe-$tRNA^{Phe}$(Cy5) at codon 2 underwent FRET with Val-$tRNA^{Val}$(Cy3) at codon 3. **(A)** Schematic of classical/hybrid equilibrium of a stalled ribosome. **(B)** Representative FRET recording**. (C)** Frames of fluctuating stalled traces formed a two-peaked distribution fitted with a double Gaussian function (n = 221 molecules). For **(D-F),** 2 µM EF-G was present during ongoing translation from codon 1 through 3. **(D)** Reaction scheme for ongoing translation, **(E)** a representative trace with the following FRET states: **(i)** the POST state after the ribosome has translated through the 1st (fMet) and 2nd (Phe) codons, with peptidyl-$tRNA^{Phe}$ residing in the P-site; **(ii, iii)** the $INT_{ongoiung}$ state and the initial POST state, which have similar FRET efficiencies (Chen et al., 2011); and **(iv)** the POST state following dissociation of $tRNA^{Phe}$(Cy5) from the E-site. **(F)** Frames of traces during ongoing translation formed a peaked PRE state distribution fitted with a single Gaussian component (n = 254 molecules).

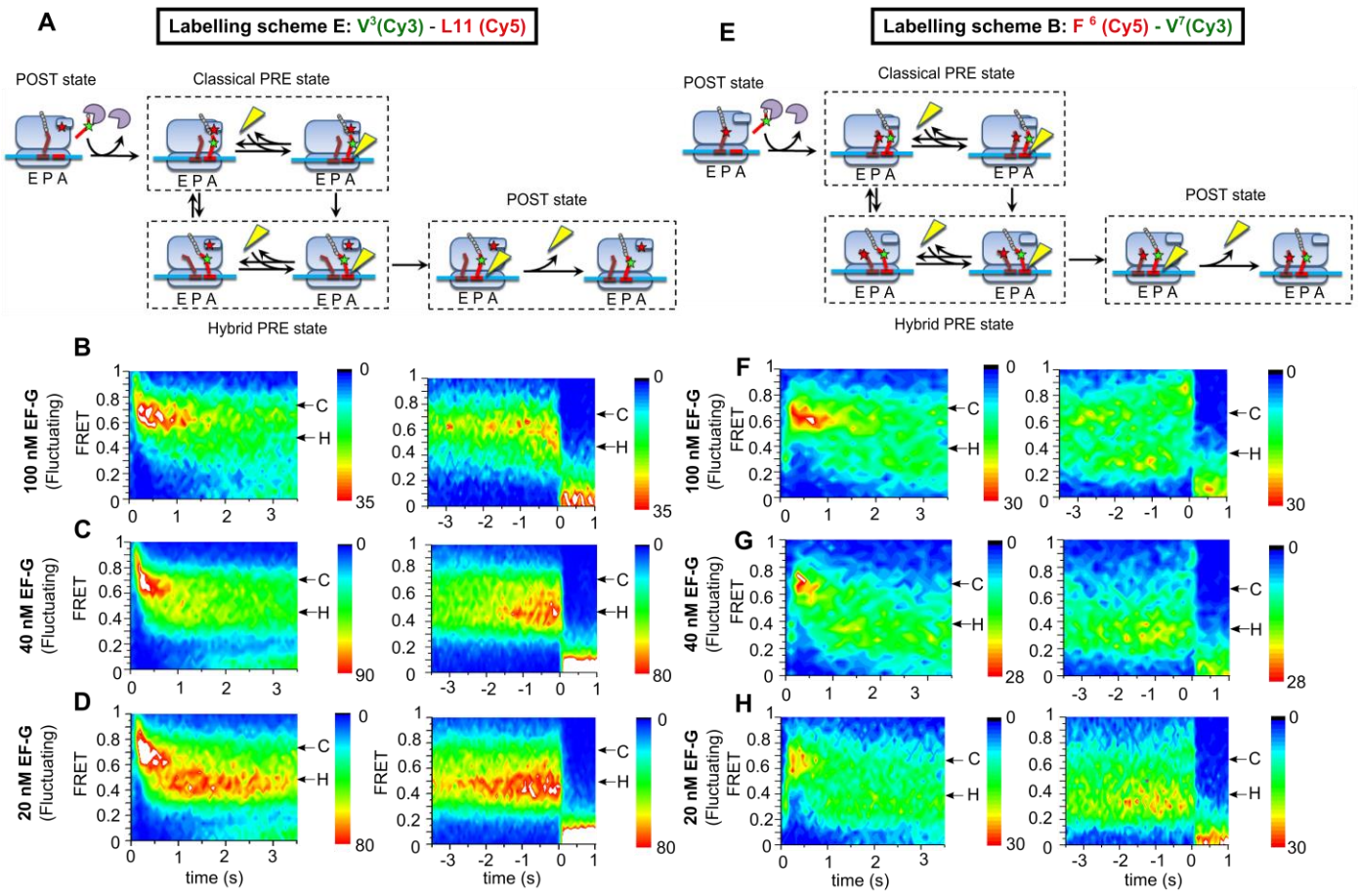

Figure S10. tRNA-L11 and tRNA-tRNA FRET at low EF-G concentration. At 20 nM to 100 nM EF-G during ongoing translation, a minority of the traces fluctuated between classical and hybrid states before translocating, despite the majority adopting a non-fluctuating intermediate FRET efficiency. **(A, E)** Reaction schemes indicating EF-G binding to either the classical or hybrid state to catalyze translocation. Pre- and post- synchronized contour maps for tRNA-L11 **(B-D)** and tRNA-tRNA **(F-H)** FRET demonstrate that at reduced EF-G concentrations, the hybrid state is more prominent and becomes the primary state from which translocation occurs.

	FRET Efficiency, Ongoing	σ_F, Ongoing	FRET Efficiency, Stalled Classical tRNA Position	σ_F, Stalled Classical	FRET Efficiency, Stalled Hybrid tRNA Position	σ_F, Stalled Hybrid
V^7(Cy3) - L11(Cy5), (Fig. 1C,F)	0.65	0.12	0.73	0.08	0.49	0.11
F^6(Cy5) - V^7(Cy3), (Fig. 2C,F)	0.58	0.16	0.68	0.10	0.39	0.12
F^6(Cy3) - V^7(Cy5) (Fig. S2C,F)	0.57	0.16	0.73	0.12	0.40	0.15
F^6(Cy3)-L11(Cy5), (Fig. S3C,F)	0.69	0.09	0.73	0.09	0.43	0.12
V^3(Cy3) - L11(Cy5), (Fig. S4C,F)	0.66	0.12	0.73	0.09	0.46	0.11
V^3(Cy5) - L11(Cy3) (Fig. S5C,F)	0.63	0.14	0.70	0.08	0.49	0.14
F^2(Cy3)-L11(Cy5), (Fig. S6C,F)	0.68	0.09	0.74	0.09	0.43	0.13

Supplemental Table 1: FRET efficiency distribution peak centers and standard deviations.

	Stalled: High FRET					
FRET pair	τ_{fast}	Proportion fast	τ_{slow}	Proportion slow	τ_{av}	Dwell time histogram
V^7(Cy3) - L11(Cy5)	0.46 s	0.63	1.59 s	0.37	0.87 s	Fig. S3A
F^6(Cy5) - V^7(Cy3)	0.35 s	0.74	1.18 s	0.26	0.56 s	Fig. S3D
F^6(Cy3)-L11(Cy5)	0.39 s	0.70	1.37 s	0.30	0.68 s	Fig. S3G
V^3(Cy3) - L11(Cy5)	0.35 s	0.75	1.01 s	0.25	0.54 s	Fig. S3G
F^2(Cy3)-L11(Cy5)	0.30 s	0.88	1.46 s	0.12	0.44 s	Fig. S1M

	Stalled: Low FRET					
FRET pair	τ_{fast}	Proportion fast	τ_{slow}	Proportion slow	τ_{av}	Dwell time histogram
V^7(Cy3) - L11(Cy5)	0.13 s	0.48	2.27 s	0.52	1.24 s	Fig. S3B
F^6(Cy5) - V^7(Cy3)	0.09 s	0.26	2.56 s	0.74	0.88 s	Fig. S3E
F^6(Cy3)-L11(Cy5)	0.14 s	0.24	2.13 s	0.76	1.66 s	Fig. S3H
V^3(Cy3) - L11(Cy5)	0.15 s	0.30	1.67 s	0.70	1.28 s	Fig. S3K
F^2(Cy3)-L11(Cy5)	0.25 s	0.69	3.27 s	0.31	1.27 s	Fig. S3N

	Ongoing Translation (+2 μM EF-G·GTP)					
FRET pair	τ_{fast}	Proportion fast	τ_{slow}	Proportion slow	$\tau_{weighted}$	Dwell time histogram
V^7(Cy3) - L11(Cy5)	0.51 s	0.31	2.33 s	0.69	1.76 s	Fig. S3C
F^6(Cy5) - V^7(Cy3)	0.36 s	0.35	2.56 s	0.64	2.08 s	Fig. S3F
F^6(Cy3)-L11(Cy5)	0.21 s	0.47	2.22 s	0.53	1.28 s	Fig. S3I
V^3(Cy3) - L11(Cy5)	0.20 s	0.21	2.50 s	0.79	1.69 s	Fig. S3L
F^2(Cy3)-L11(Cy5)	0.11 s	0.61	3.04 s	0.39	1.28 s	Fig. S3O

Supplemental Table 2: Dwell times PRE states for stalled and ongoing experiments calculated by fitting double exponential decays to the unbinned dwell time data using maximum likelihood estimation as described in the Supplemental Methods, and plotted in Fig. S7. τ_{av} is the weighted average dwell time calculated using Eq. S5 in Supplemental Methods.

FRET pair	Fraction of ongoing traces observed to transition to the canonical hybrid state	Fraction of ongoing traces predicted to transition to the hybrid state based on kinetic rates observed in stalled ribosomes (Suppl. Eq. S6)
V^7(Cy3) - L11(Cy5)	184 / 3664 = 0.050	0.65
F^6(Cy5) - V^7(Cy3)	100 / 2359 = 0.042	0.75
F^6(Cy3) - V^7(Cy5)	10 / 200 = 0.050	0.49
F^6(Cy3)-L11(Cy5)	11 / 1423 = 0.008	0.55
V^3(Cy3) - L11(Cy5)	74 / 2157 = 0.034	0.65
V^3(Cy5) - L11(Cy3)	18 / 319 = 0.056	0.58
F^2(Cy3)-L11(Cy5)	10 / 434 = 0.025	0.50

Supplemental Table 3: Fraction of ongoing ribosome populations expected to undergo classical to hybrid transitions based on stalled fluctuation dwell times.

FRET pair	$\frac{1}{k_{high\rightarrow low} + k_{low\rightarrow high}}$ from weighted dwell times of fluctuating stalled ribosomes	τ_{decay} from cross-correlation as a function lag for fluctuating stalled ribosomes
V^7(Cy3) - L11(Cy5)	0.51 s	0.52 s
F^6(Cy5) - V^7(Cy3)	0.34 s	0.31 s

Supplemental Table 4: τ_{decay} from exponential fitting of cross-correlation as a function of lag (Supp. Eq. S7) for fluctuating stalled ribosomes (Fig. S8E,G), compared to the expected rate constant calculated from the sum of the classical and hybrid FRET tRNA position dwell times.

As the mentioned in the main text, stalled fluctuating traces had strongly anti-correlated donor and acceptor intensities as expected for FRET intensities during fluctuations in distance. Ongoing traces did not (Fig. S8E,G) exhibit anti-correlated FRET signals, thus ruling out fluctuations slower than 30 s^{-1}. This analysis can be extended by calculating the cross-correlation as a function of lag in the time domain. Also called a "sliding inner product" or cross-correlogram, the two signals are shifted in time with respect to each other before calculating the cross-correlation for each amount of shift (Supp. Eq. S7), a technique commonly used in signal processing to search a long noisy signal for a shorter or encoded feature, or to determine the time delay between signals (Lathi, 2004). In this context, a shift of integer numbers of camera frames between donor and acceptor intensities reduces positive or negative correlations towards zero, since stochastic changes of the two channels' intensities become out of sync as they are shifted relative to each other. In fact, the negative cross-correlation of the stalled traces decayed to zero at a rate consistent with the sum its kinetic constants ($k_{classic\rightarrow hybrid} + k_{hybrid\rightarrow classic}$) as expected (Guttfreund, 1995). In contrast, the positive cross-correlation of the ongoing translation intensities decayed to zero within one frame of lag (Fig. S8E,G), consistent with common-mode noise (e.g. laser intensity fluctuations), rather than rapid distance fluctuations.

Supplemental Experimental Procedures

mRNA sequences

5'-biotin- mRNA (Dharmacon, Inc.) had the following sequences:

FVR at beginning of message, mRNA-2,3: biotin-AUU UAA AAG UUA AUA AGG AUA CAU ACU *AUG UUC GUG CGU UAU UAU UAU UAU UAU UAU UAU UAU UAU.* The italicized sequence codes for amino acids MFVRYYYYYYYYY.

FVR several codons into message, mRNA-6.7: biotin-AUU UAA AAG UUA AUA AGG AUA CAU ACU *AUG UAU UAU UAU UAU UUC GUG CGU UAU UAU UAU UAU UAU.* The italicized sequence codes for MYYYYFVRYYYYY.

The underlined sequence is a strong Shine-Dalgarno region.

Initiation complex formation

Double variant C38S/S87C-L11 was constructed via site-directed mutagenesis of the N-terminal His-tagged L11 used previously (Qin et al., 2009; Seo et al., 2006; Wang et al., 2007), expressed and labeled with Cy5-maleimide (GE) as previously described (Chen et al., 2011). To reconstitute L11 ribosomes, a 2-fold molar excess of C38S/S87C-L11Cy5 was incubated with 2 µM AM77 70S ribosomes lacking L11 in TAM_{15} buffer (50 mM Tris- HCl [pH 7.5], 15 mM $Mg(OAc)_2$, 30 mM NH_4Cl, 70 mM KCl, 1 mM DTT) (Chen et al., 2011)) with 5 mM additional $Mg(OAc)_2$ for 15 min at 37 °C. The reconstituted ribosomes then underwent ultracentrifugation as previously described (Qin et al., 2009; Wang et al., 2007). 70S initiation complex was formed by incubating 1 µM 70S ribosomes, 4 µM biotin-mRNA (sequences listed above), 1.5 µM each of IF1, IF2, IF3 and fMet-$tRNA^{fMet}$, and 1 mM GTP in TAM_{15} buffer for 25 min at 37 °C.

tRNAs and ternary complex formation

tRNAs were prepared using the reduction and charging protocols previously described (Chen et al., 2011; Pan et al., 2009) starting with *E. coli* $tRNA^{fMet}$, $tRNA^{Tyr}$, $tRNA^{Val}$, and yeast $tRNA^{Phe}$ purchased from Chemical Block (Moscow). $tRNA^{Phe}$ and $tRNA^{Val}$ were with Cy3, and $tRNA^{Val}$ with Cy5, via a dihydroU-hydrazine linkage as described (Kaur et al., 2011). Ternary complex was formed by incubating 4 µM EF-Tu, 2 µM dye-labeled and charged tRNA, 3 mM GTP, 1.3 mM phosphoenolpyruvate, and 5 µg/mL pyruvate kinase in TAM_{15} buffer for 15 min at 37 °C.

Flow chamber construction

The sample flow chambers (8 µL) were formed on slides with holes drilled using a 1.25 mm diamond-tipped drill bit. Double-sided tape laid between the drilled holes served as spacers and separated the flow chambers. Polyethylene tubing with 0.97 mm outer diameter (Warner Instruments) was inserted into each hole and sealed with 5 min epoxy. The coverslips were then sealed in place via the double-sided tape and epoxy at their edges. These flow chambers allow fast injection of reaction mixtures into the channels while recording image series.

smFRET: General conditions

smFRET studies were carried out at 23 °C in TAM_{15} buffer . An enzymatic deoxygenation system of 0.3% (w/v) glucose, 300 µg/ml glucose oxidase (Sigma-Aldrich), 120 µg/ml catalase (Roche), and 1.5 mM 6-hydroxy-2,5,7,8-tetramethyl-chromane-2-carboxylic acid (Trolox, Sigma-Aldrich) was added to TAM_{15} to form the final imaging buffer to reduce fluorophore photobleaching and blinking (Chen et al., 2011). Microscope slides and coverslips were coated with polyethylene glycol (m-PEG-SVA-2000; Laysan Bio) to prevent nonspecific binding, as well as 1-5% biotinylated-PEG (biotin-PEG-SC-2000; Laysan Bio, (Roy et al., 2008)), and flow chambers were constructed as described above. 0.5 mg/ml Streptavidin was applied to the surface and washed away with TAM_{15} buffer before 1 - 5 nM initiation complex was added and immobilized on the surface via biotin-mRNA. Unbound initiation complex was washed away with TAM_{15} buffer. Image stacks were recorded on a custom-built objective-type total internal reflection fluorescence (TIRF) microscope based on a commercial inverted microscope (Eclipse Ti-E, Nikon) and equipped with the ability to perform alternating-laser excitation (ALEX) between 532 nm and 640 nm laser beams (Chen et al., 2011). For the experiments at lower Mg^{2+} concentration presented in Fig. S9, the reaction buffer contained 50 mM HEPES-KOH (pH 7.3), 4.5 mM $MgAc_2$, 4 mM 2-mercaptoethanol, 150 mM NH_4Ac, 0.05 mM spermine, 2 mM spermidine (Dinos et al., 2005).

Stalled ribosome smFRET

After immobilizing the initiation complex on the slides, solutions with 10 nM un-labeled TC, 2 µM EF-G, and 3 mM GTP in TAM_{15} were injected to allow the ribosome to translate through all of the codons preceding the codon corresponding to the tRNA. For Val-$tRNA^{Val}$(Cy3)-L11(Cy5) experiments, the codons preceding Val required un Tyr-$tRNA^{Tyr}$ and Phe-$tRNA^{Phe}$ TCs, whereas for Phe-$tRNA^{Phe}$(Cy3)-L11(Cy5) experiments, only Tyr-$tRNA^{Tyr}$ TC was required. For Phe-$tRNA^{Phe}$(Cy5)-Val-$tRNA^{Val}$(Cy3) experiments, the Phe-$tRNA^{Phe}$(Cy5) TC was injected along with the un-labeled Tyr-$tRNA^{Tyr}$ ternary complex; thus the P-site was occupied with Cy5- $tRNA^{Phe}$ in the POST state.

The unbound ternary complex and EF-G were then washed out with TAM_{15} buffer, and the vacant A-sites of the ribosomes were filled by injecting 10 nM cognate TC, forming a stalled PRE state. Finally, unbound ternary complex was washed out by TAM_{15} buffer with imaging buffer, and image stacks were acquired at 35 ms per frame using ALEX illumination, resulting in a net 70 ms time resolution. For the experiments observing PRE complex formation in real time, the un-labeled cognate ternary complex was injected while recording 35 ms frames with only 532 nm laser illumination.

Ongoing translation smFRET
After the initiation complex was immobilized on the slides via biotin-streptavidin linkage as described above, unbound initiation complex was washed out with TAM_{15} buffer. While recording image stacks, imaging buffer solution was injected containing 2 μM EF-G, 3 mM GTP, 10 nM Tyr-tRNA^{Tyr} ternary complex, and 10 nM each of Phe-tRNA^{Phe} TC and Val-tRNA^{Val} TC (labeled or un-labeled depending on the experiment). Ongoing translation experiments were recorded with 532 nm excitation at 35 ms time resolution.

Calculation of FRET efficiency
FRET efficiency was calculated according to (Ha et al., 1999):

$$E = \left(1 + \frac{I_D}{I_A - \chi I_D}\gamma\right)^{-1} = \frac{(I_A - \chi I_D)}{(I_A - \chi I_D) + \gamma I_D} \qquad \text{(S1)}$$

where I_D and I_A are the raw fluorescence intensities of the donor and acceptor, χ is the cross-talk of the donor emission into the acceptor recording channel, and γ accounts for the ratios of quantum yield and detection efficiency between the donor and the acceptor channels. Based on bootstrapping with 1000 iterations, the 95% confidence intervals for the peaks of the FRET efficiency distributions are all <0.005.

Compensating FRET efficiencies for 532 nm excitation of Cy5
The excitation spectrum for Cy5 includes a small component at 532 nm, leading to a very low amount of direct excitation of Cy5 by the 532 nm laser. For ongoing translation experiments with Cy3- tRNAs arriving at ribosomes already containing a Cy5- L11 subunit or Cy5- tRNA in the P-site, that excitation of Cy5 at 532 nm was taken into account by zeroing the very low sensitized acceptor intensity immediately before the event began. Subsequently, the FRET efficiency during ongoing translation can be directly calculated according to Equation S1. However, for the stalled traces in which the PRE complex was formed before the recording began, zeroing the acceptor intensity to eliminate that component was not possible.

To quantitatively compare the stalled traces to ongoing traces, a correction factor φ representing this cross-excitation was calculated using the stalled traces in which Cy3 bleached before Cy5:

$$\varphi = \frac{I_{A,after\ event}}{\left(I_{A,during\ event} - \chi I_{D,during\ event}\right) + \gamma I_{D,during\ event}} \qquad \text{(S2)}$$

Values of φ formed distributions that were fitted with single Gaussian components, and the corresponding peak center values were used to calculate FRET efficiency as follows:

$$E = \frac{I_A - \chi I_D - \varphi(I_A - \chi I_D + \gamma I_D)}{I_A - \chi I_D - \varphi(I_A - \chi I_D + \gamma I_D) + \gamma I_D} \qquad \text{(S3)}$$

This cross-excitation correction reduced the reported peak FRET efficiencies of the stalled classical and hybrid tRNA positions by approximately 0.02.

Photobleaching
The dwell times for the PRE state during ongoing translation (Fig. S3) were much shorter than the bleaching times of the fluorophores. Thus a Val-tRNA^{Val}(Cy3) – L11(Cy5) experiment with alternating 532/640 nm laser excitation (ALEX) showed that 83% of the traces translocated before photo-bleaching (Fig. S1). This result is consistent with the 85-88% predicted for the entire population of ongoing FRET events based on the photobleaching times while using ALEX (8.4-14 s), in which the acceptor (Cy5) bleaches first in >90% of traces. If the analysis is restricted to the most biologically significant fast phase subpopulation, the percentage of ribosomes translocating before photobleaching is even higher (94-98%). The direct excitation of the acceptor by the 640 nm laser during ALEX experiments accelerated the rate of photobleaching. Thus, the percentages given above of ribosomes that translocate before photobleaching are lower limits for experiments using only 532 nm illumination.

Hidden Markov model analysis of smFRET traces
Image stacks were converted to intensity recordings using an ImageJ plugin written in-house (Chen et al., 2011). FRET traces were analyzed by Hidden Markov Model-based software (HaMMy)(McKinney et al., 2006); for the stalled traces no more than two FRET states were identified by the program in any of the individual traces, and recordings with two FRET states were termed fluctuating traces. Ongoing traces were analyzed by the same program, which identified multiple states in a very small proportion (1% – 4%) of recordings at 2 μM EF-G (Table S3), but which did find more fluctuating examples at lower EF-G concentrations (Fig. 3C,F, S10).

Selection of stalled ribosome smFRET traces
To determine the high and low FRET values associated with the classical and hybrid tRNA positions of stalled ribosomes, only ribosomes fluctuating between two FRET states (as identified by HaMMy) were used. That population is enriched for higher

translational activity; approximately 80% of the ribosomes identified as fluctuating are capable of translocating after the injection of EF-G, whereas less than 25% of ribosomes that do not fluctuate while stalled complete translocation (Chen et al., 2011).

Dwell time fitting and comparison with fluctuation rates

Dwell times for each of the states were poorly fit by single exponential decays. Double exponential functions of the form

$$\frac{C}{\tau_{fast}} e^{-\frac{t}{\tau_{fast}}} + \frac{(1-C)}{\tau_{slow}} e^{-\frac{t}{\tau_{slow}}} \qquad \text{(S4)}$$

were fitted to unbinned dwell time data by maximum likelihood estimation (Bevington and Robinson, 2002; Woody et al., 2016), in which the probability distribution is convolved with the camera instrument response function to account for finite camera framing (Lewis et al., 2017).

The resulting fitting parameters were combined to estimate the average dwell time according to:

$$\tau_{av} = C\,\tau_{fast} + (1-C)\tau_{slow} \qquad \text{(S5)}$$

To separately analyze the FRET traces belonging to the faster component, a time threshold was determined such that that the proportion of the double exponential distribution with dwell times below the threshold matches the fraction (*C*) that the fast phase contributes to the whole distribution.

To estimate the numbers of ongoing traces that would have switched state if the ongoing FRET values were canonical classical or hybrid tRNA positions, the transition rates of these processes were compared with the observed PRE dwell time. For two competing exponential processes (fluctuation from the initial state and translocation), we seek the probability that a trace will fluctuate before translocation. Taking the dwell times for both translocation and fluctuation as double exponential decays, the probability of a fluctuation before translocation is given by:

$$P[t_f < t_d] = \int_{t_d=0}^{\infty} \int_{t_f=0}^{t_d} \left[\frac{C_f}{\tau_{f1}} e^{\frac{-t_f}{\tau_{f1}}} + \frac{(1-C_f)}{\tau_{f2}} e^{\frac{-t_f}{\tau_{f2}}}\right]\left[\frac{C_d}{\tau_{d1}} e^{\frac{-t_d}{\tau_{d1}}} + \frac{(1-C_d)}{\tau_{d2}} e^{\frac{-t_d}{\tau_{d2}}}\right] dt_f dt_d \qquad \text{(S6)}$$

Where t_f is the time until the stalled ribosome fluctuates, t_d is the time until the ongoing PRE state translocates, τ_{f1} and τ_{f2} are the fast and slow phase time constants for the classical state of fluctuating stalled ribosomes, C_f and $(1-C_f)$ are their respective contributions, τ_{d1} and τ_{d2} are the fast and slow phase time constants for the PRE state occupancy during ongoing translation, and C_d and $(1-C_d)$ are their respective contributions. Values for this probability are given in Table S3, indicating that many more ongoing ribosomes would have exhibited fluctuations than were observed if the ongoing FRET state is one of the canonical classical or hybrid tRNA positions with normal stalled ribosome transition rates.

Donor-acceptor cross-correlation

The cross-correlation, C_k, between the donor (I_d) and acceptor (I_a) intensity traces of length *n* with a lag of k frames was calculated by concatenating the donor vector with a second copy of itself and using the following equation (Weisstein, 2002), in which $\overline{I_d}$ and $\overline{I_a}$ represent the average acceptor and donor intensities of each trace, while σ_d and σ_a represent the standard deviations of those intensities throughout that trace.

$$C_k = \frac{\sum_{i=1}^{n}\left[(I_{a_{i+k}} - \overline{I_a})(I_{d_i} - \overline{I_d})\right]}{n\sigma_a\sigma_d} \qquad \text{(S7)}$$

Supplemental References

Bevington, P.R., and Robinson, D.K. (2002). Data Reduction and Error Analysis for the Physical Sciences (New York: McGraw-Hill).

Chen, C., Stevens, B., Kaur, J., Cabral, D., Liu, H., Wang, Y., Zhang, H., Rosenblum, G., Smilansky, Z., Goldman, Y.E., et al. (2011). Single-molecule fluorescence measurements of ribosomal translocation dynamics. Mol. Cell *42*, 367–377.

Dinos, G., Kalpaxis, D.L., Wilson, D.N., and Nierhaus, K.H. (2005). Deacylated tRNA is released from the E site upon A site occupation but before GTP is hydrolyzed by EF-Tu. Nucleic Acids Res. *33*, 5291–5296.

Geggier, P., Dave, R., Feldman, M.B., Terry, D.S., Altman, R.B., Munro, J.B., and Blanchard, S.C. (2010). Conformational sampling of aminoacyl-tRNA during selection on the bacterial ribosome. J. Mol. Biol. *399*, 576–595.

Guttfreund, H. (1995). Kinetics for the life sciences: receptors, transmitters, and catalysts (Cambridge: Cambridge University Press).

Ha, T., Ting, A.Y., Liang, J., Caldwell, W.B., Deniz, A.A., Chemla, D.S., Schultz, P.G., and Weiss, S. (1999). Single-molecule fluorescence spectroscopy of enzyme conformational dynamics and cleavage mechanism. Proc. Natl. Acad. Sci. U. S. A. *96*, 893–898.

Kaur, J., Raj, M., and Cooperman, B.S. (2011). Fluorescent labeling of tRNA dihydrouridine residues : Mechanism and distribution. 1393–1400.

Lathi, B.P. (2004). Linear Signals and Systems (Oxford University Press).

Lewis, J.H., Jamiolkowski, R.M., Woody, M.S., Ostap, E.M., and Goldman, Y.E. (2017). Deconvolution of Camera Instrument Response Functions. Biophys. J. *112*, 1214–1220.

McKinney, S.A., Joo, C., and Ha, T. (2006). Analysis of Single-Molecule FRET Trajectories Using Hidden Markov Modeling. Biophys. J. *91*, 1941–1951.

Pan, D., Qin, H., and Cooperman, B.S. (2009). Synthesis and functional activity of tRNAs labeled with fluorescent hydrazides in the D-loop. RNA *15*, 346–354.

Qin, H., Grigoriadou, C., and Cooperman, B.S. (2009). Interaction of IF2 with the Ribosomal GTPase-Associated Center during 70S Initiation Complex Formation. Biochemistry *48*, 4699–4706.

Roy, R., Hohng, S., and Ha, T. (2008). A practical guide to single-molecule FRET. Nat Meth *5*, 507–516.

Seo, H.-S., Abedin, S., Kamp, D., Wilson, D.N., Nierhaus, K.H., and Cooperman, B.S. (2006). EF-G-Dependent GTPase on the Ribosome. Conformational Change and Fusidic Acid Inhibition†. Biochemistry *45*, 2504–2514.

Wang, Y., Qin, H., Kudaravalli, R.D., Kirillov, S. V, Dempsey, G.T., Pan, D., Cooperman, B.S., and Goldman, Y.E. (2007). Single-molecule structural dynamics of EF-G--ribosome interaction during translocation. Biochemistry *46*, 10767–10775.

Weisstein, E.W. (2002). CRC Concise Encyclopedia of Mathematics (Boca Raton: CRC Press).

Woody, M.S., Lewis, J.H., Greenberg, M.J., Goldman, Y.E., and Ostap, E.M. (2016). MEMLET: An Easy-to-Use Tool for Data Fitting and Model Comparison Using Maximum-Likelihood Estimation. Biophys. J. *111*, 273–282.